

Supporting Information

Multifunctionalization of cellulose microfibrils through a cascade pathway entailing the sustainable Passerini Multi-Component reaction

Asja Pettignano,^a Julien Leguy,^b Laurent Heux,^b Bruno Jean,^b Aurélia Charlo,^{a*}, Etienne Fleury^{a*}

^a Université de Lyon, INSA LYON, Ingénierie des Matériaux Polymères IMP-UMR CNRS 5223 F 69621, Villeurbanne, France

^b Université Grenoble Alpes, CERMAV, F-38000, Grenoble, France

*Corresponding authors: aurelia.charlot@insa-lyon.fr, etienne.fleury@insa-lyon.fr

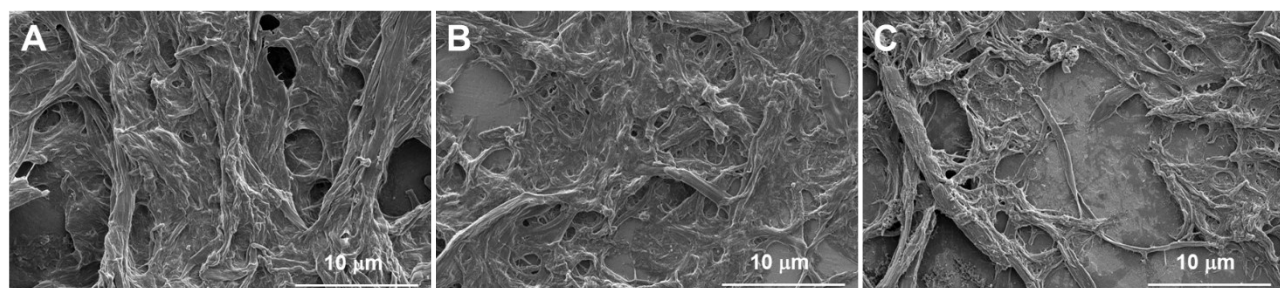
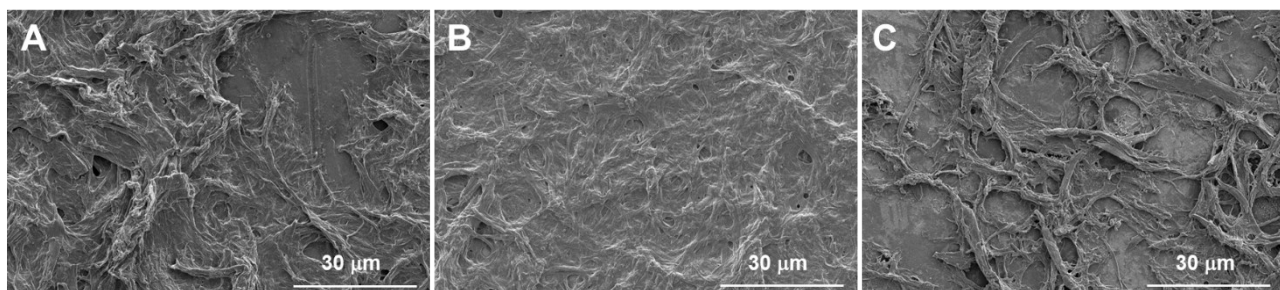


Fig. S1. SEM micrographs from dried suspensions of A) unmodified POC, DO = 0.77, B) POC_{0.77}-Pent-*t*B (Table 1, Entry 4) and C) POC_{0.77}-MA-*t*B (Table 1, Entry 11). Scale bar: 30 μm, and 10 μm.

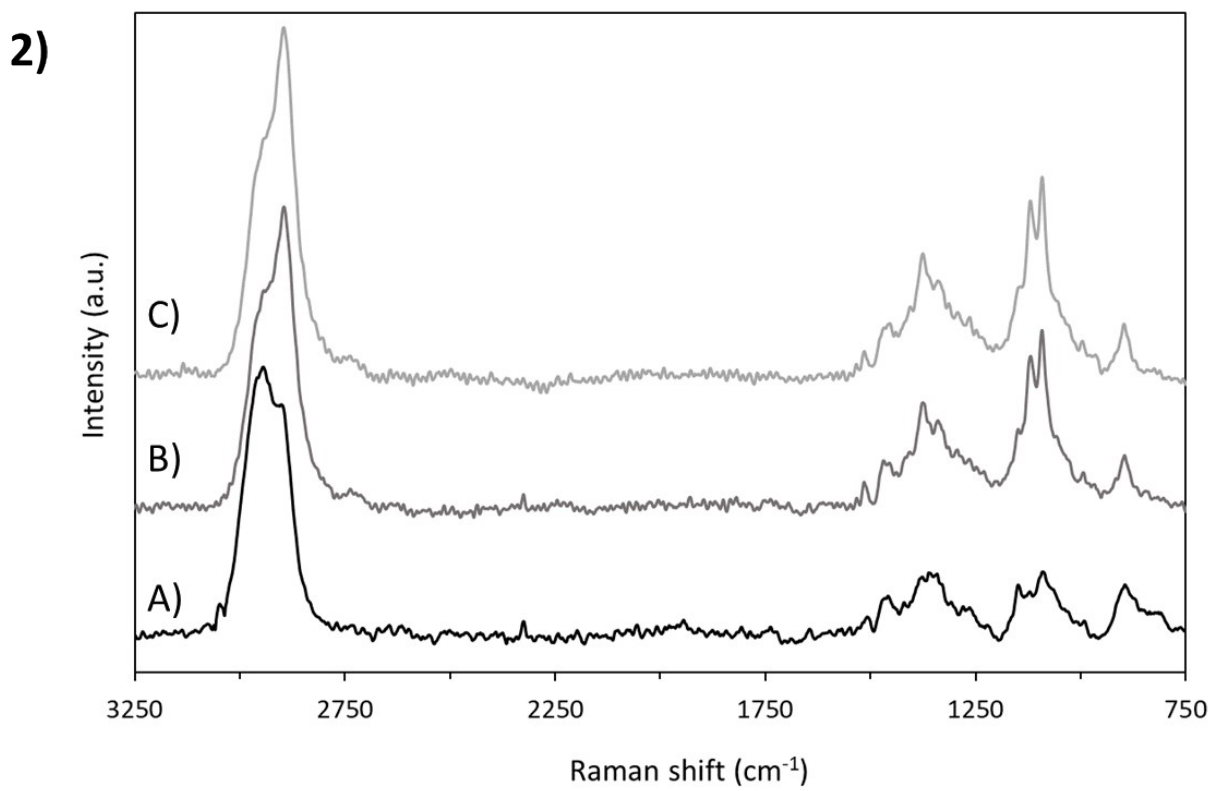
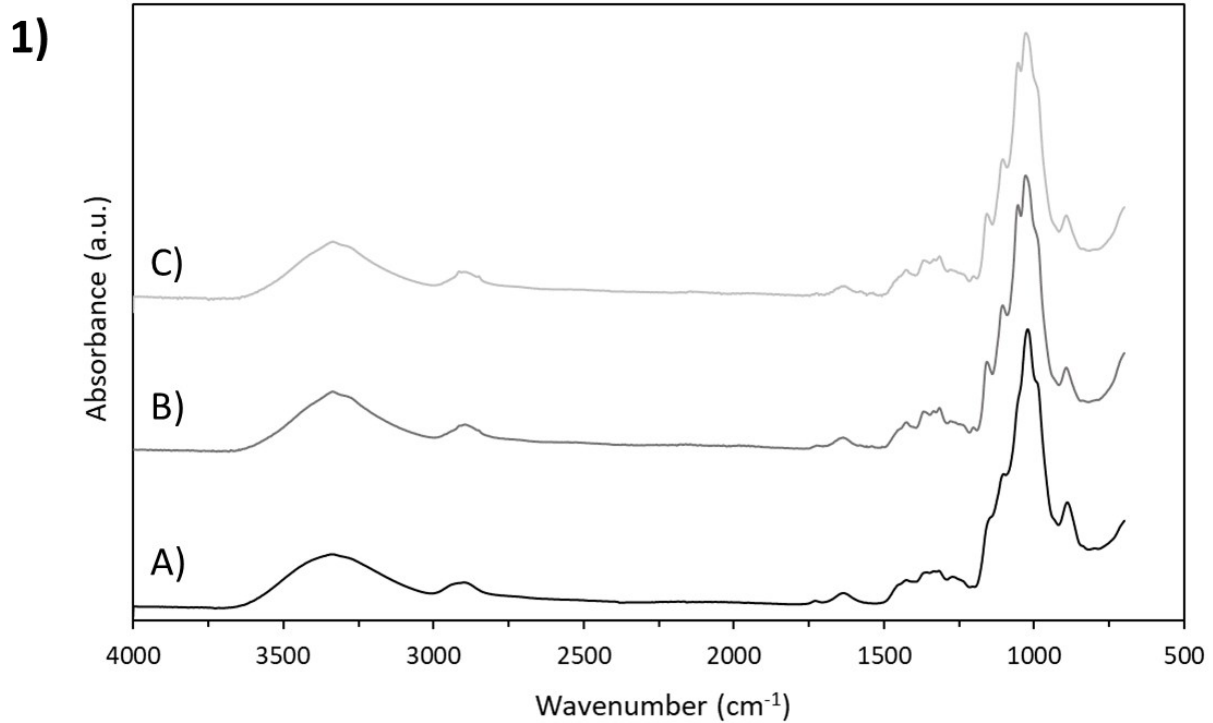
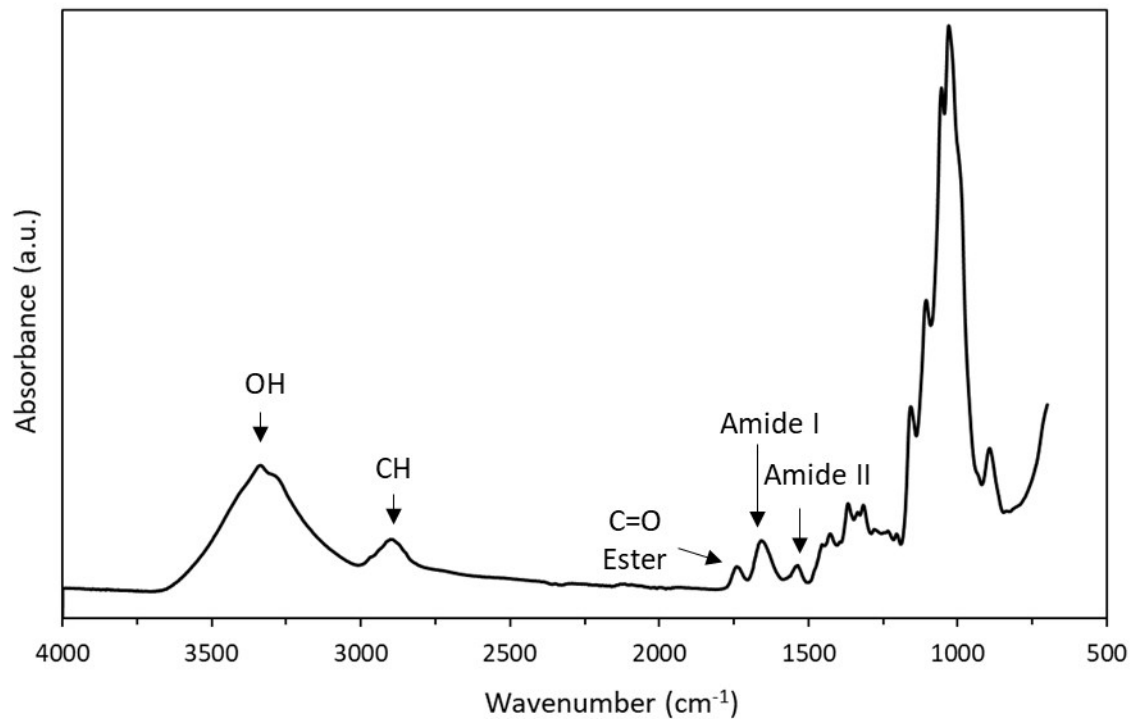
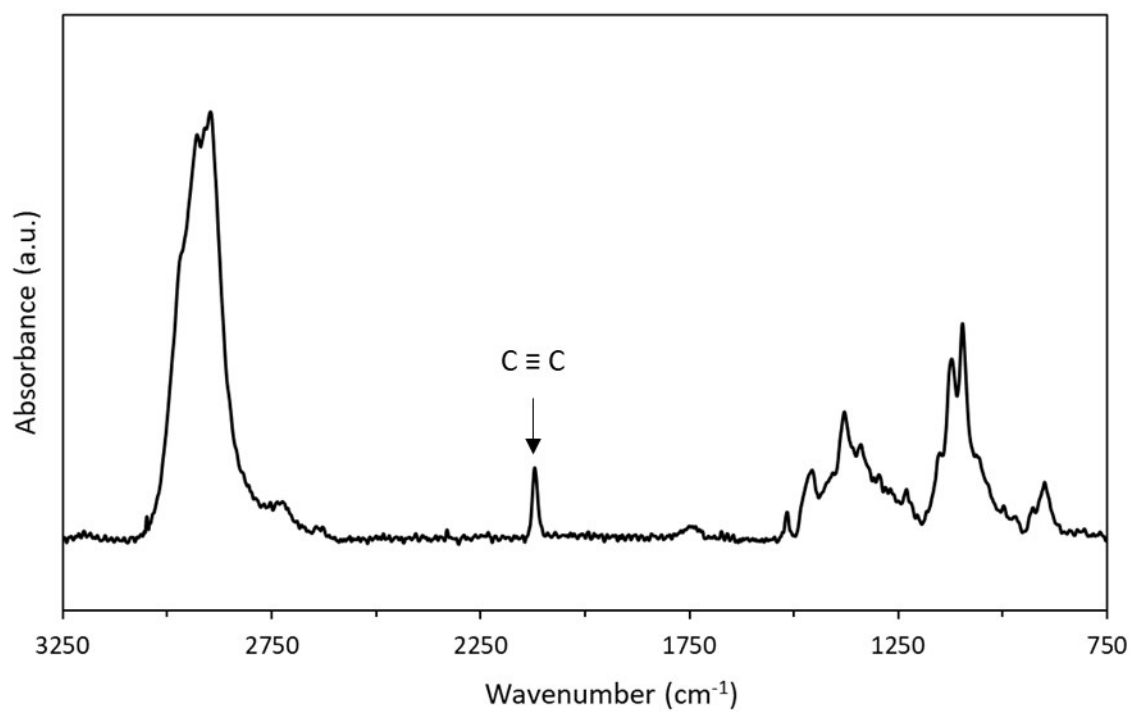


Fig. S2. ATR-IR (1) and Raman (2) spectra of unmodified POC, DO = 0.77 (A, —), blank reaction between POC (DO = 0.77) and pentynoic acid (B, —) and between POC (DO = 0.77) and methacrylic acid (C, —).

A)



B)



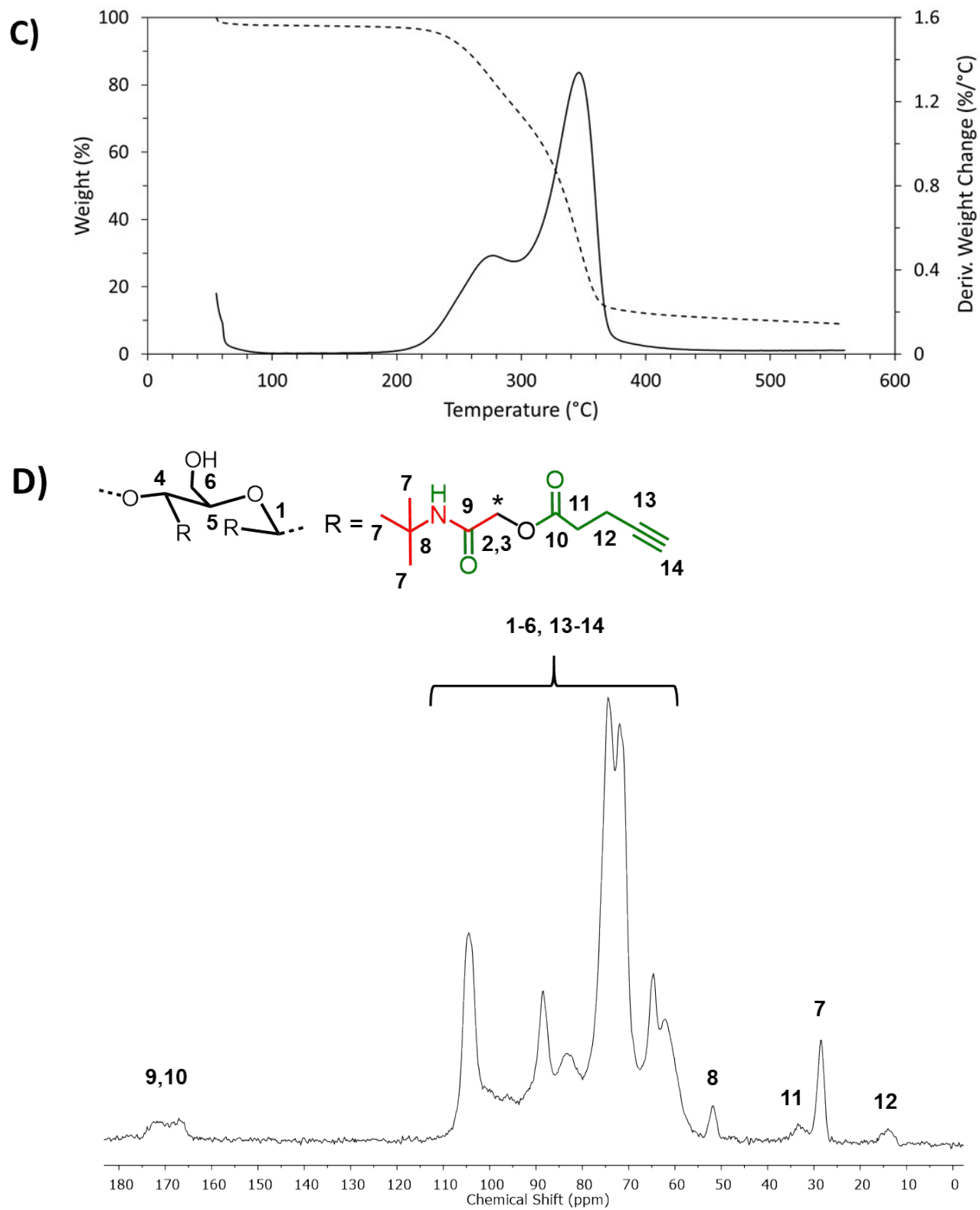
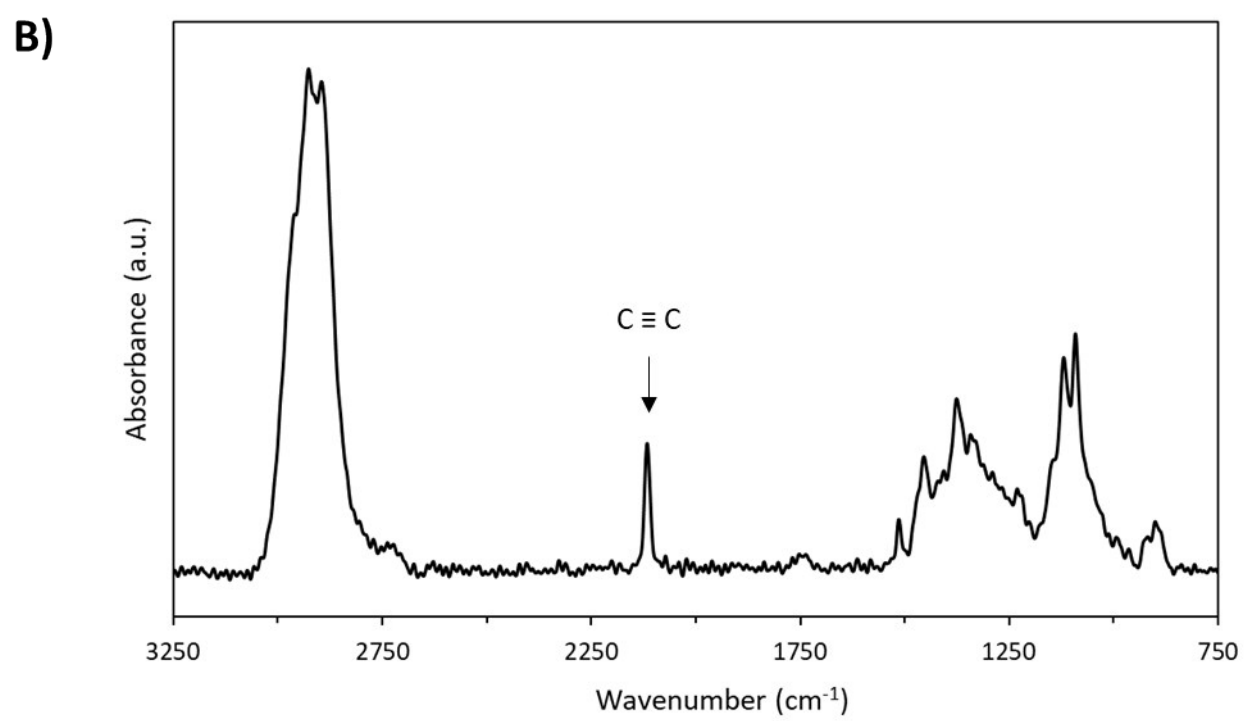
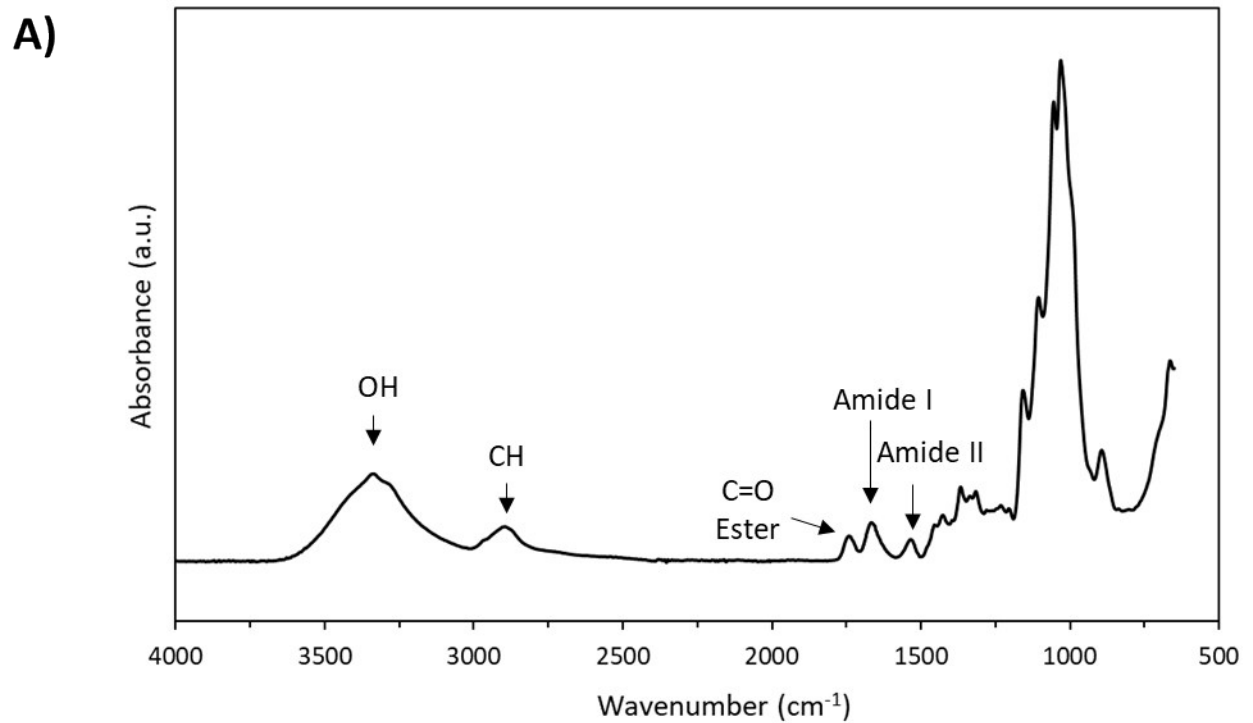


Fig. S3. A) ATR-IR, B) Raman, C) TGA and D) ^{13}C CP-MAS of Entry 1 (Table 1).



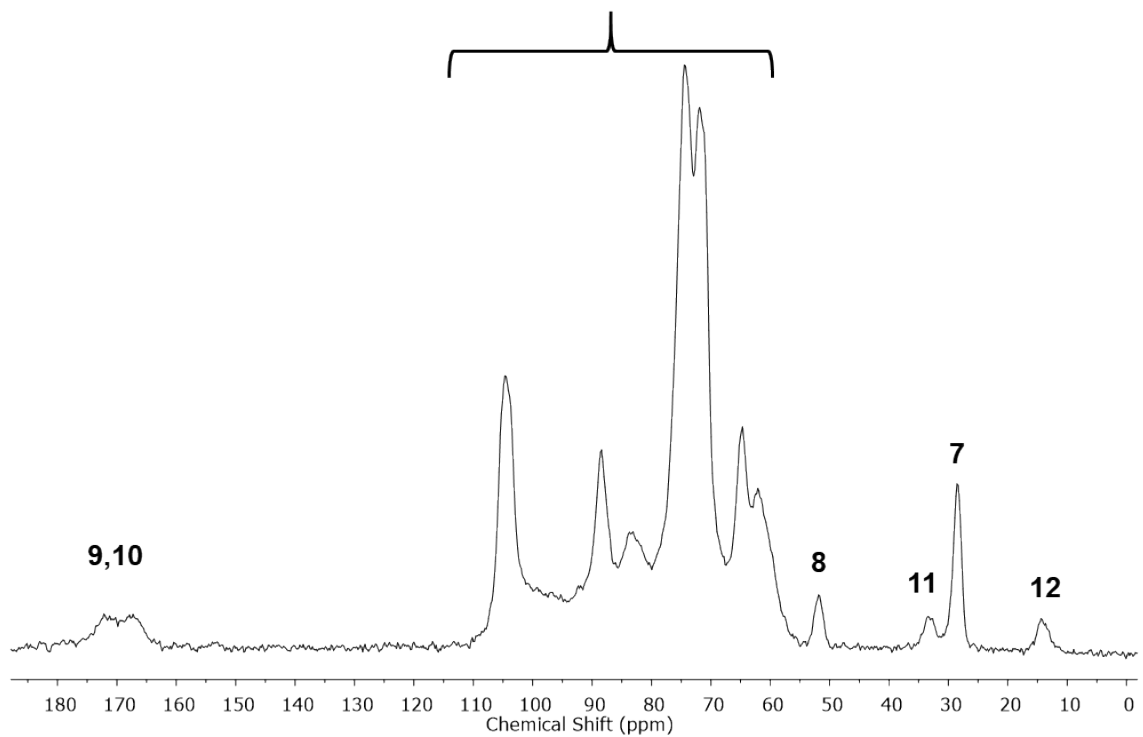
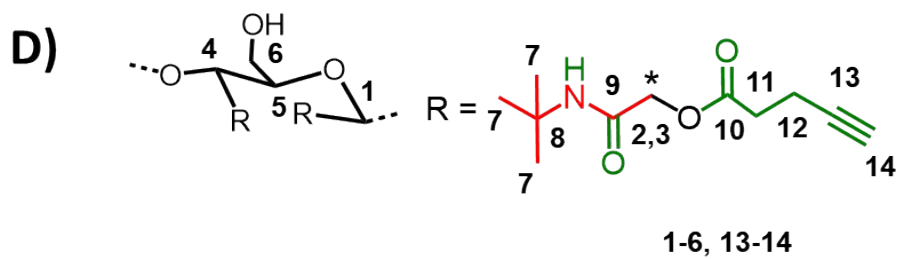
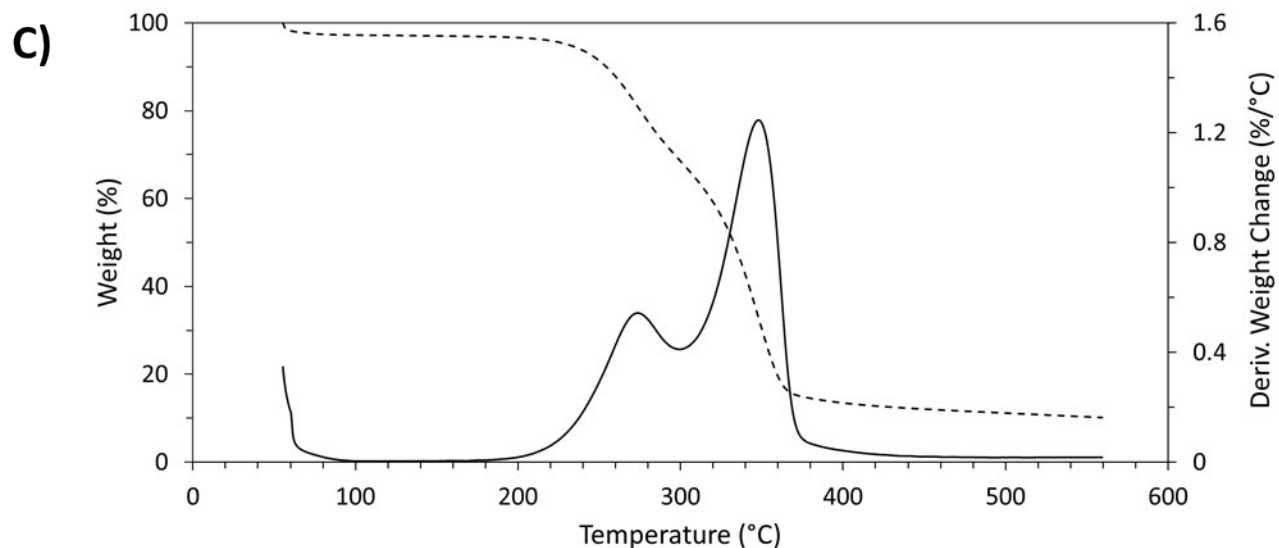
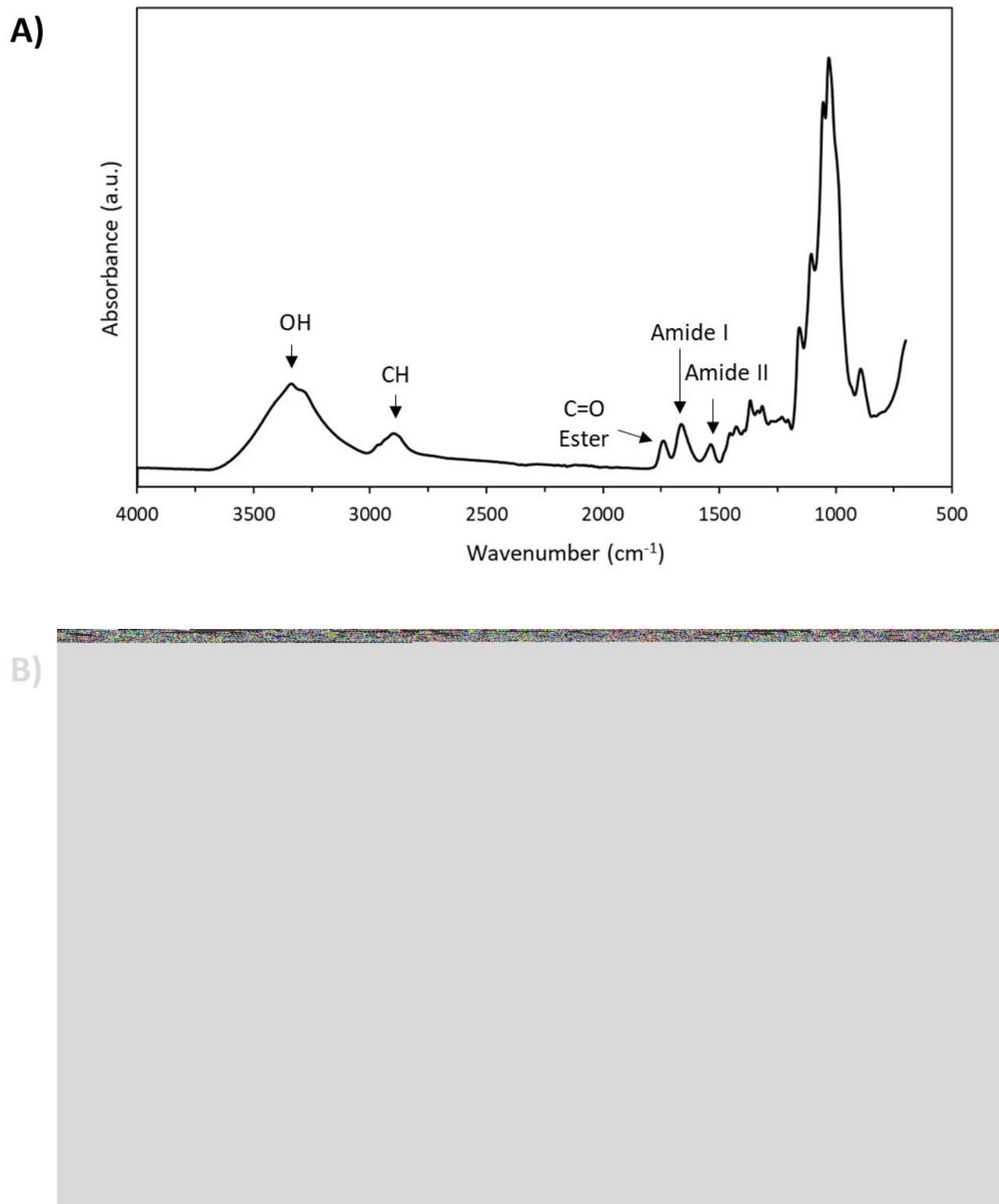


Fig. S4. A) ATR-IR, B) Raman, C) TGA and D) ^{13}C CP-MAS of Entry 2 (Table 1).



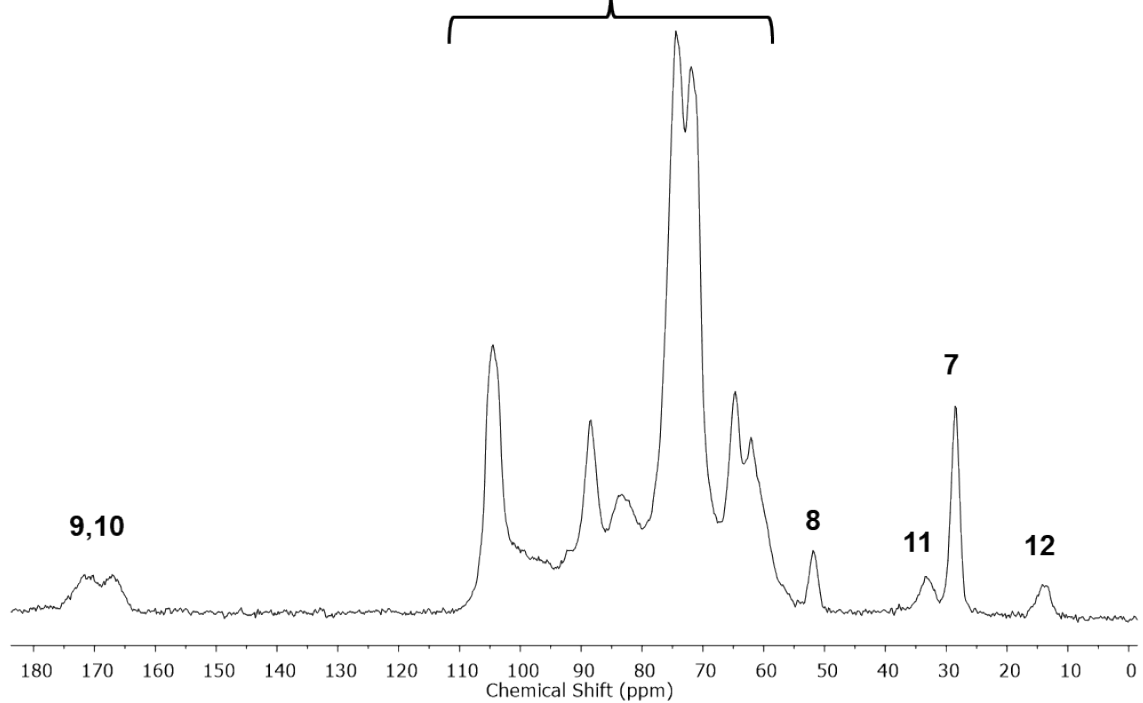
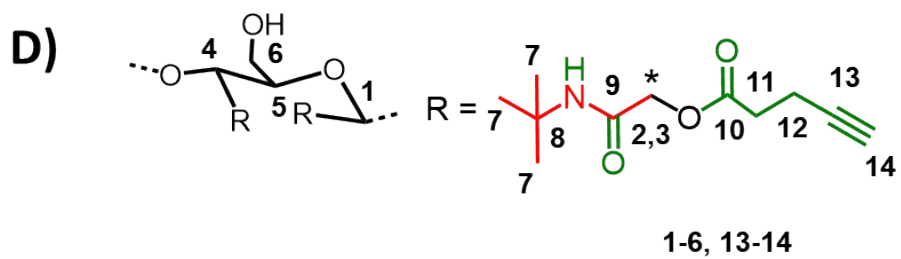
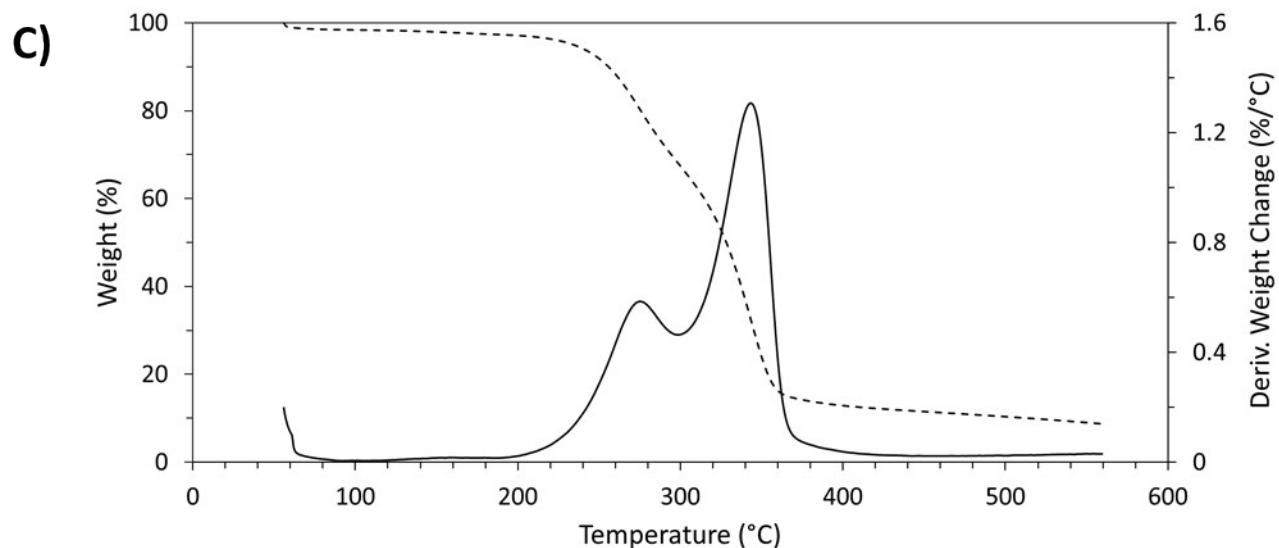
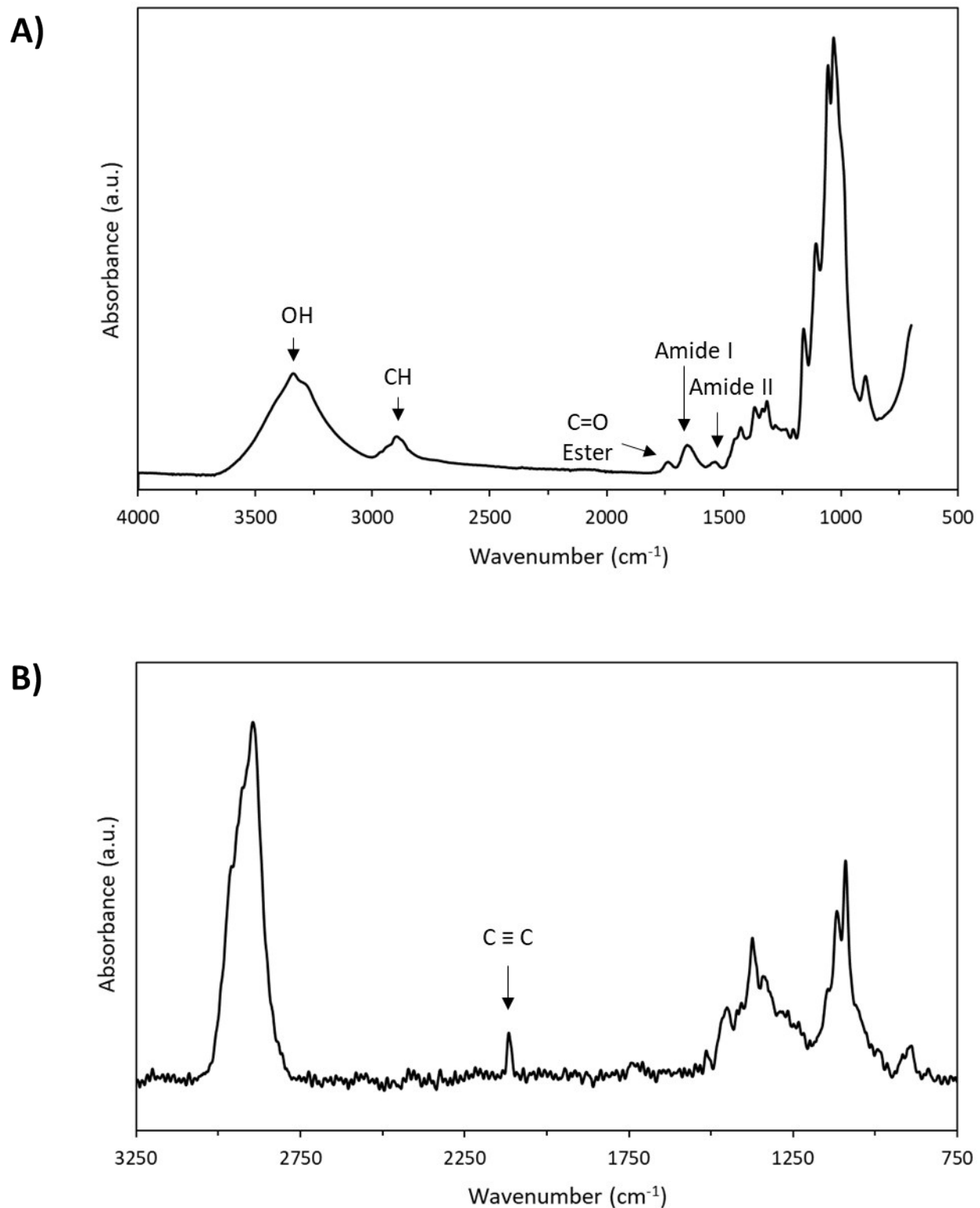
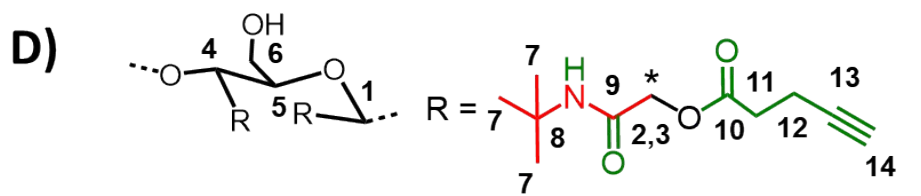
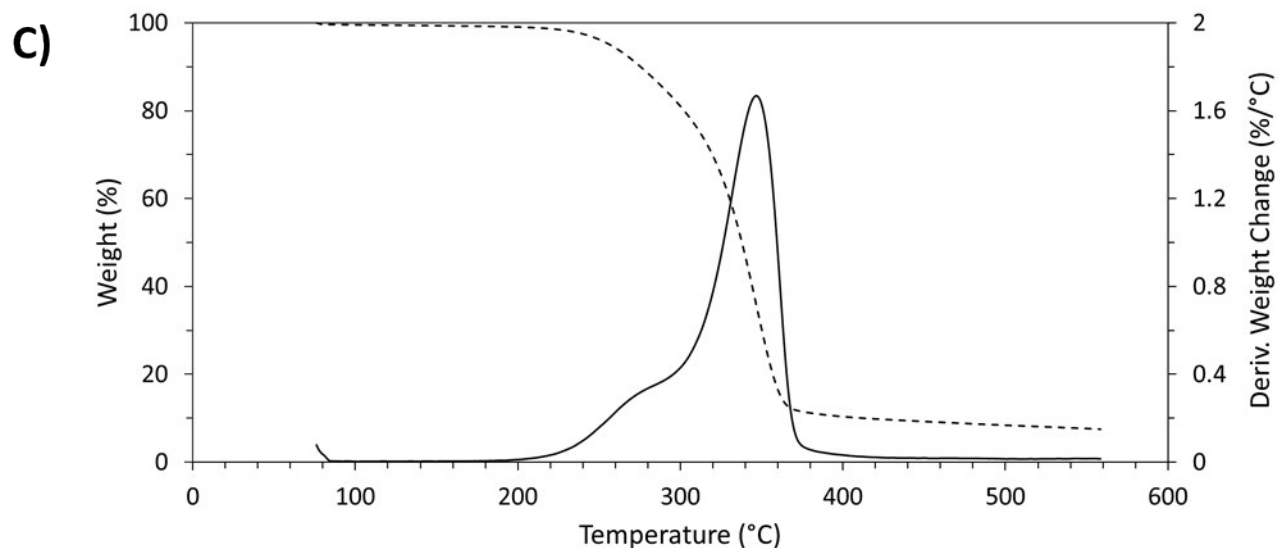


Fig. S5. A) ATR-IR, B) Raman, C) TGA and D) ^{13}C CP-MAS of Entry 3 (Table 1).





1-6, 13-14

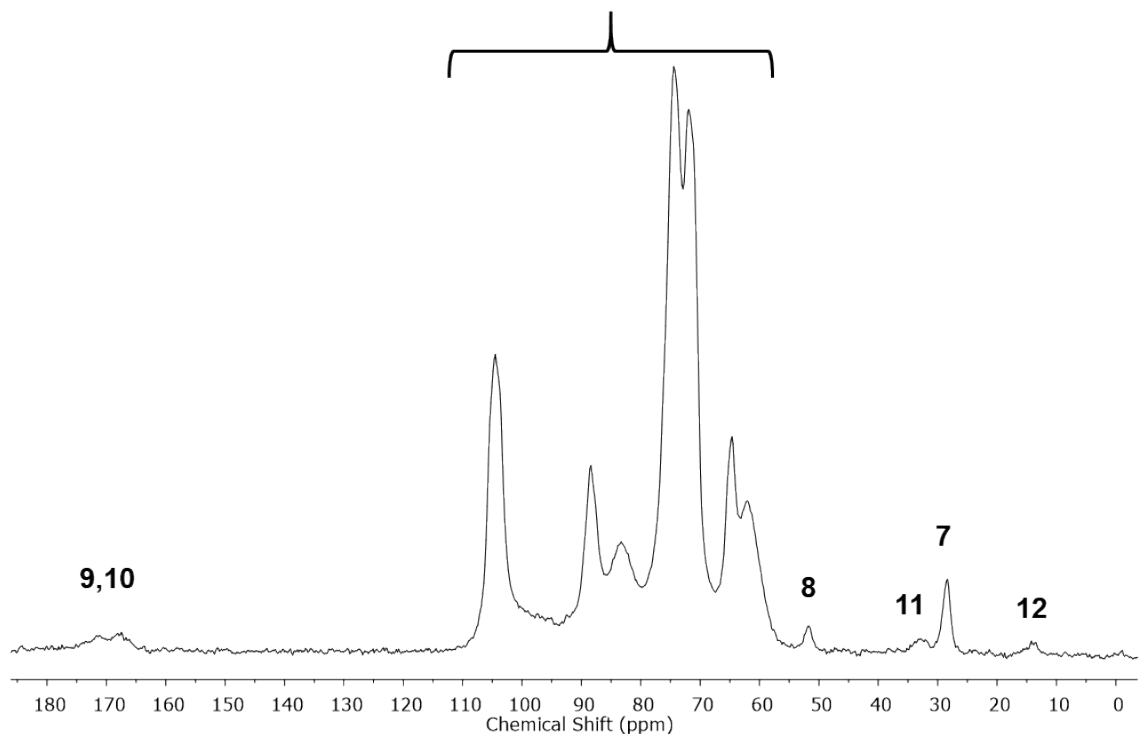
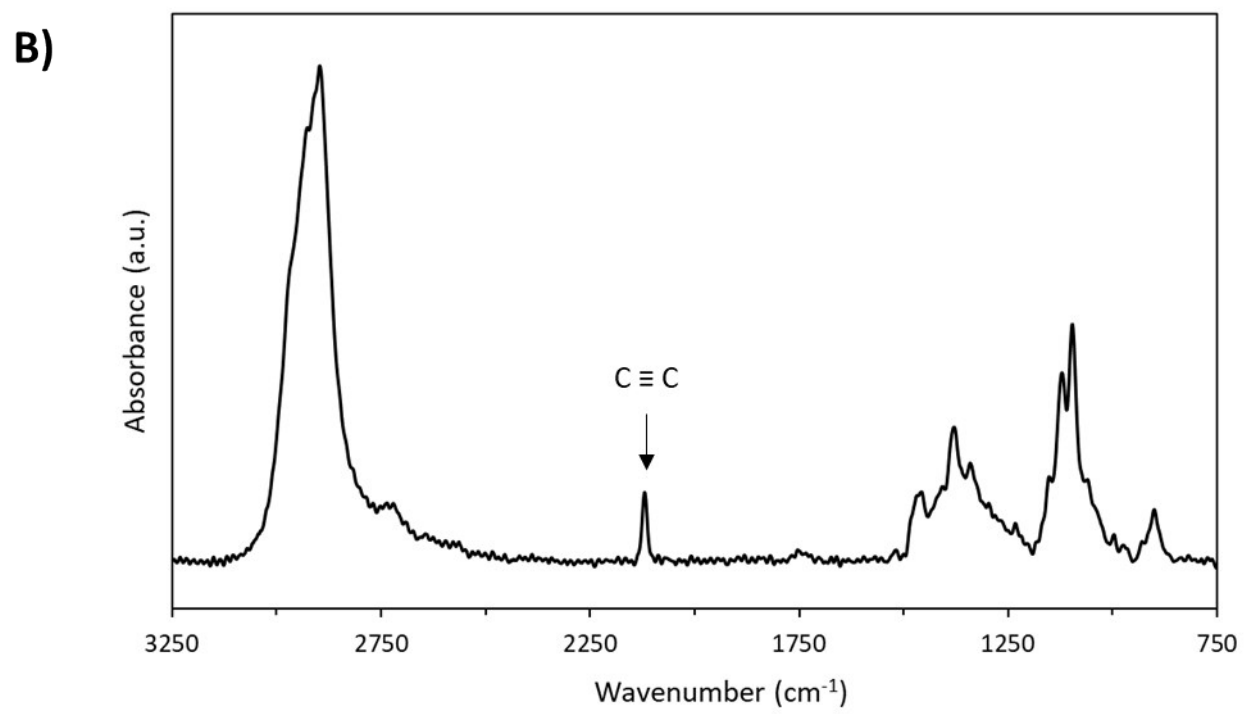
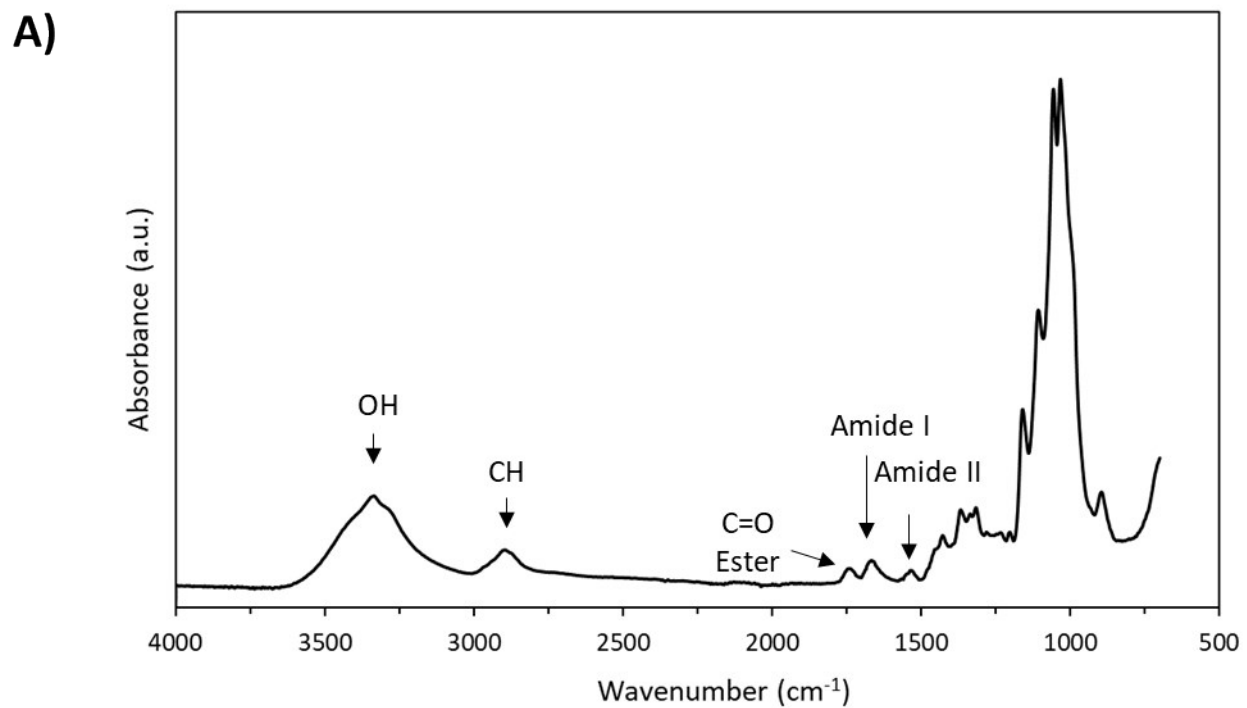


Fig. S6. A) ATR-IR, B) Raman, C) TGA and D) ¹³C CP-MAS of Entry 5 (Table 1).



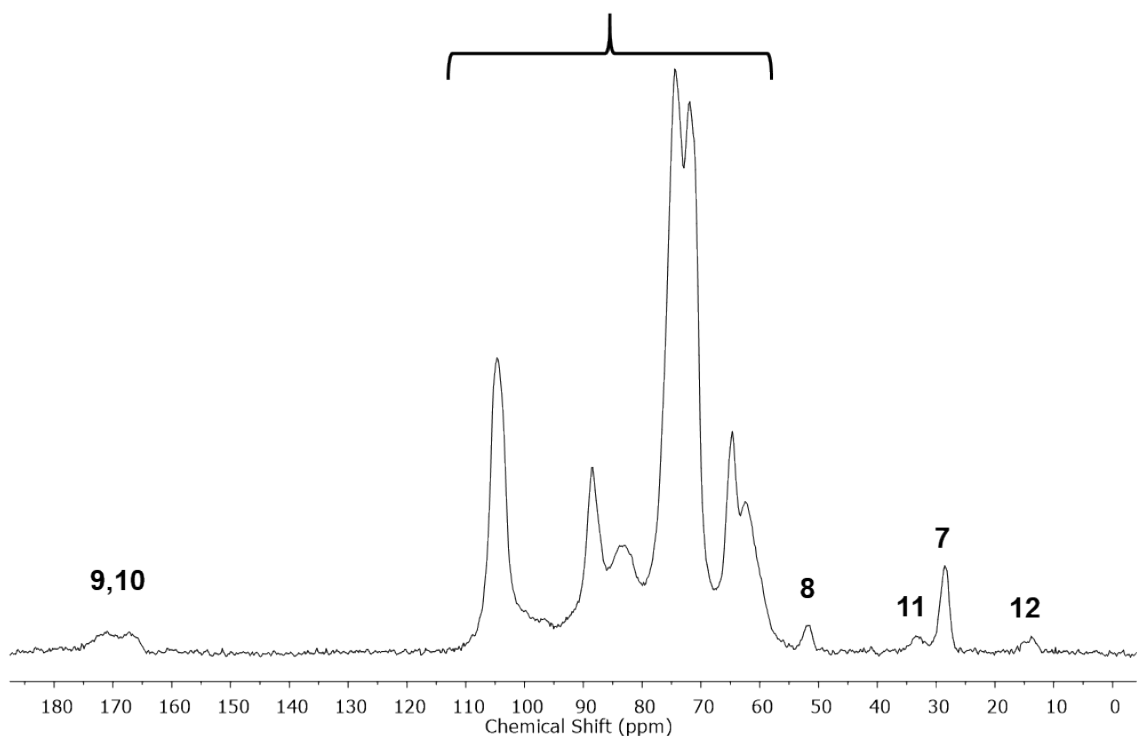
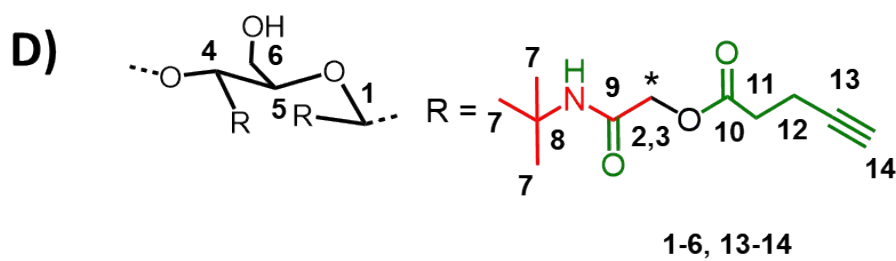
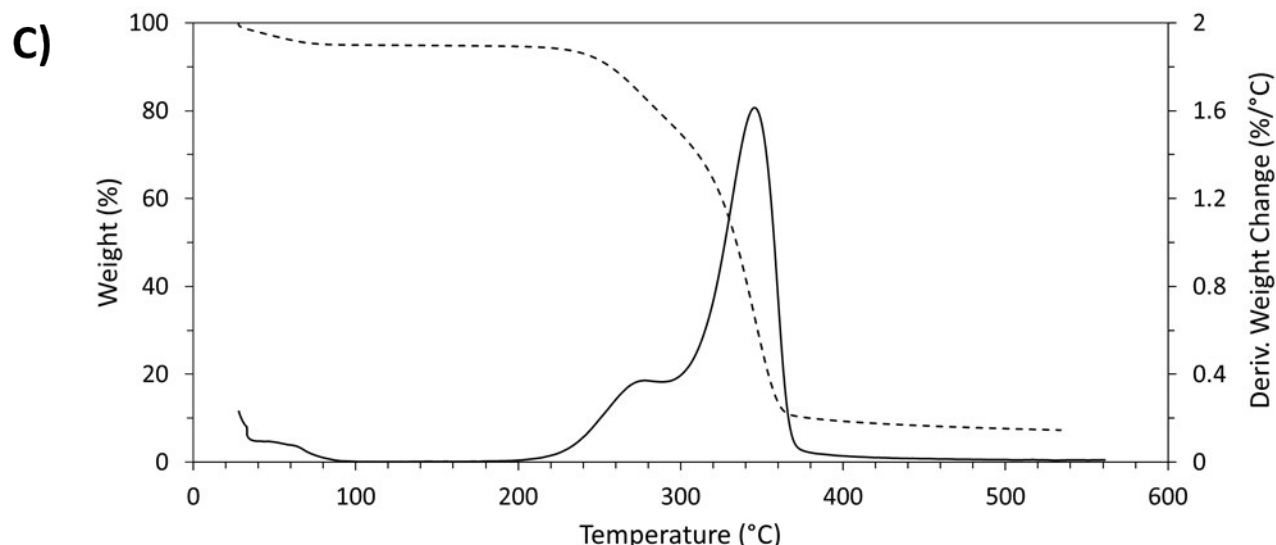
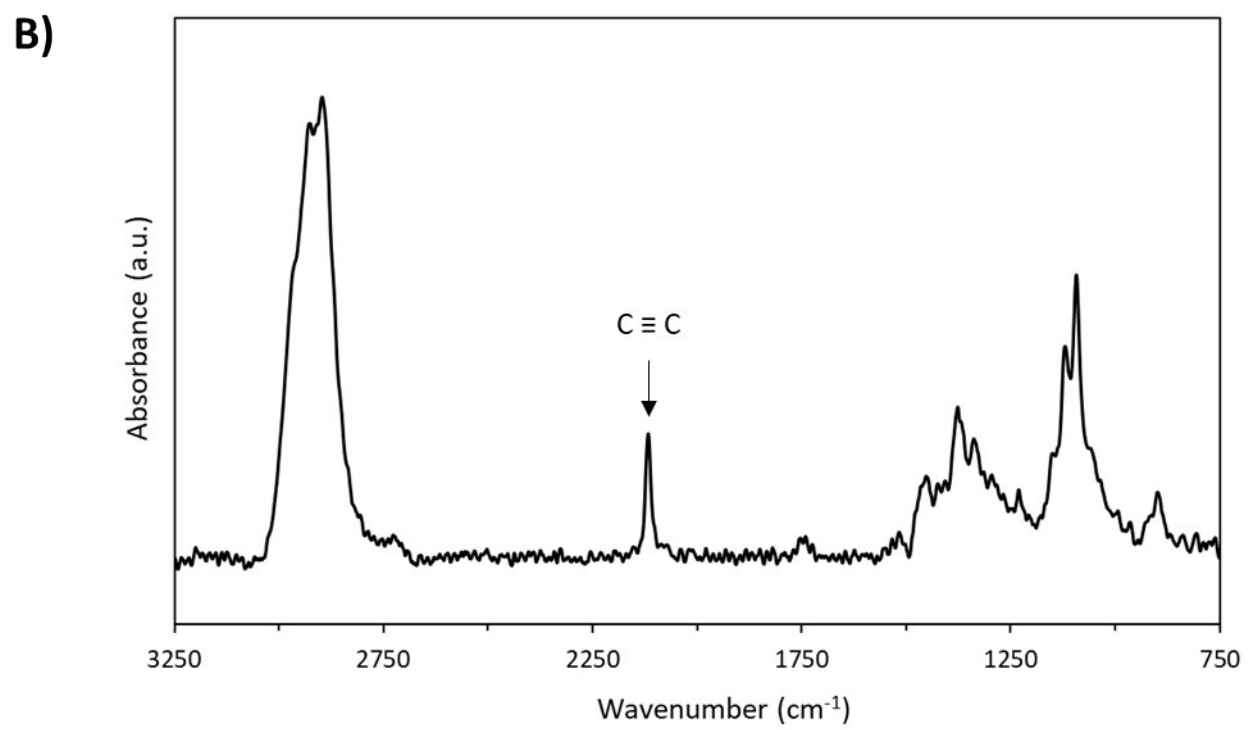
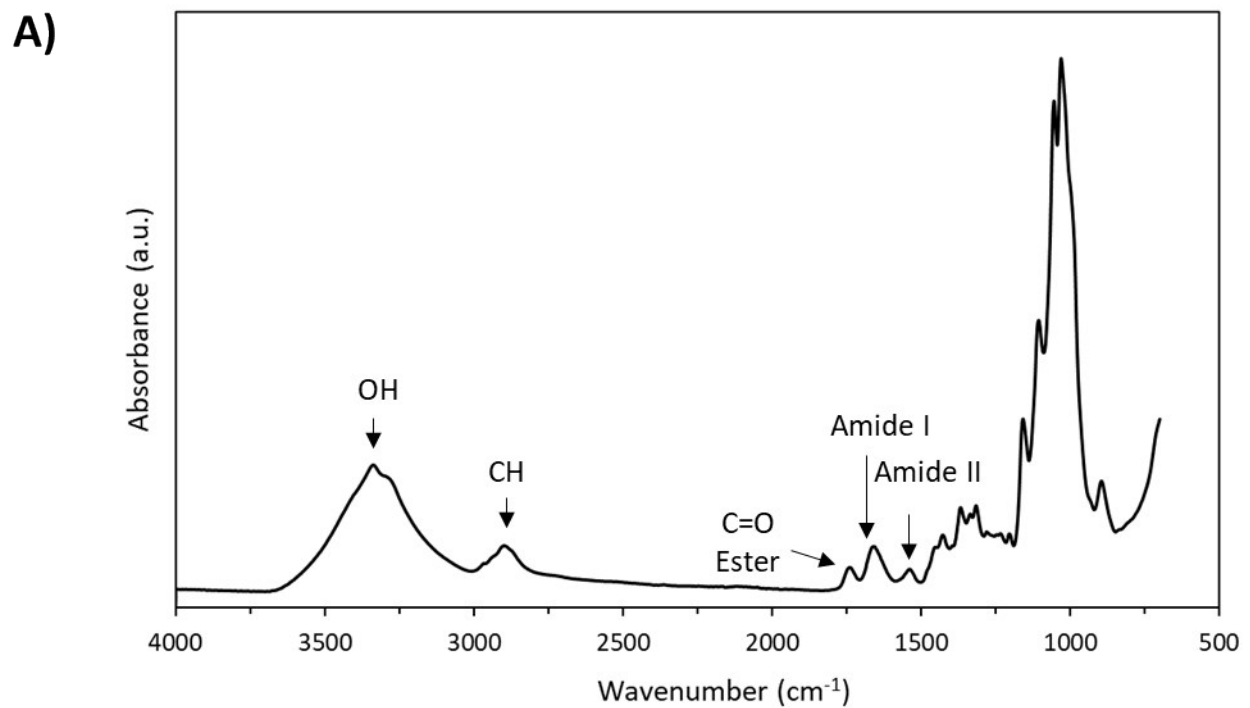


Fig. S7. A) ATR-IR, B) Raman, C) TGA and D) ^{13}C CP-MAS of Entry 6 (Table 1).



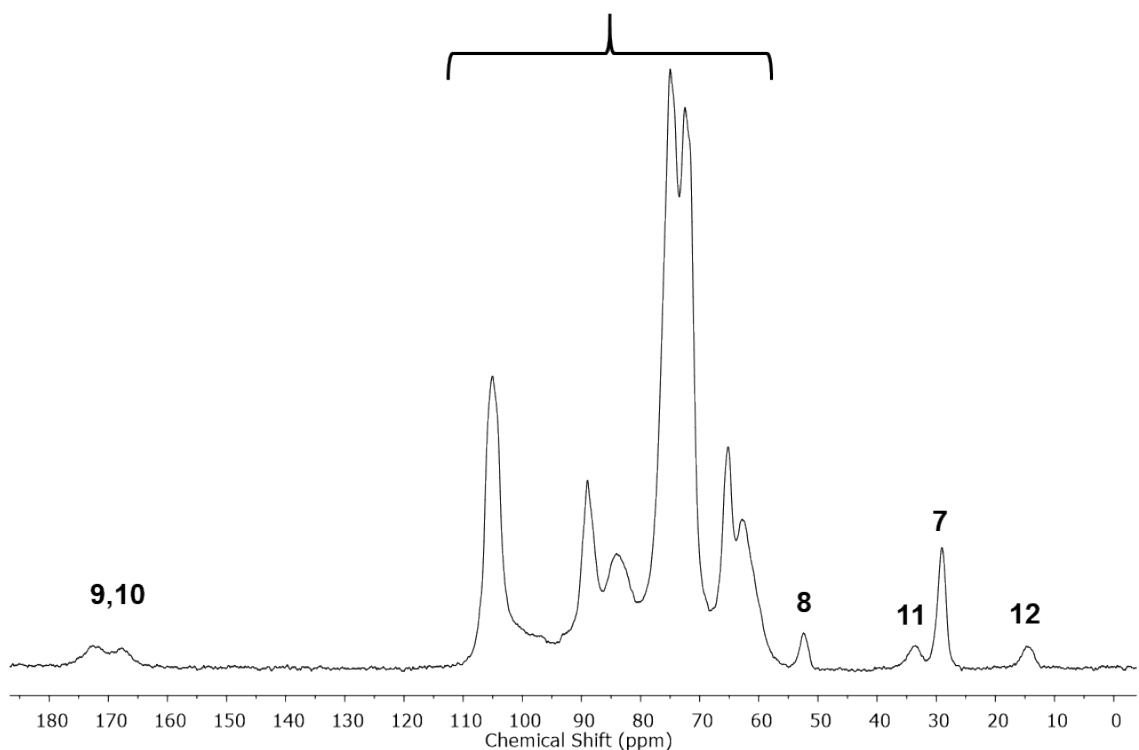
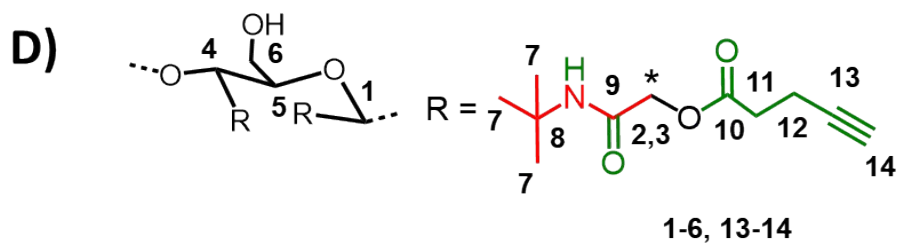
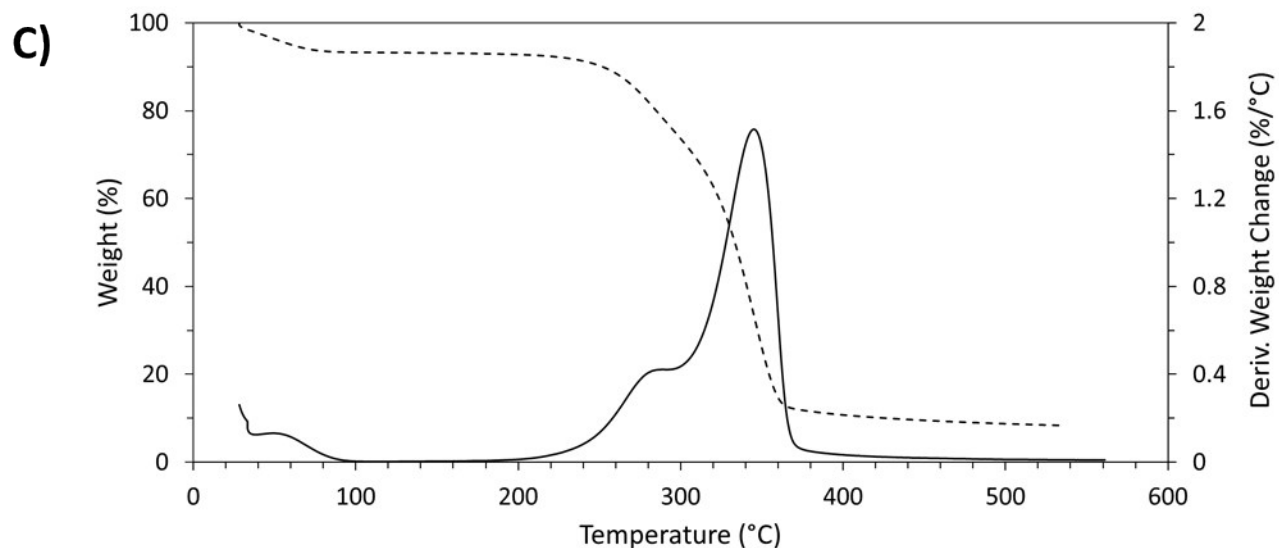
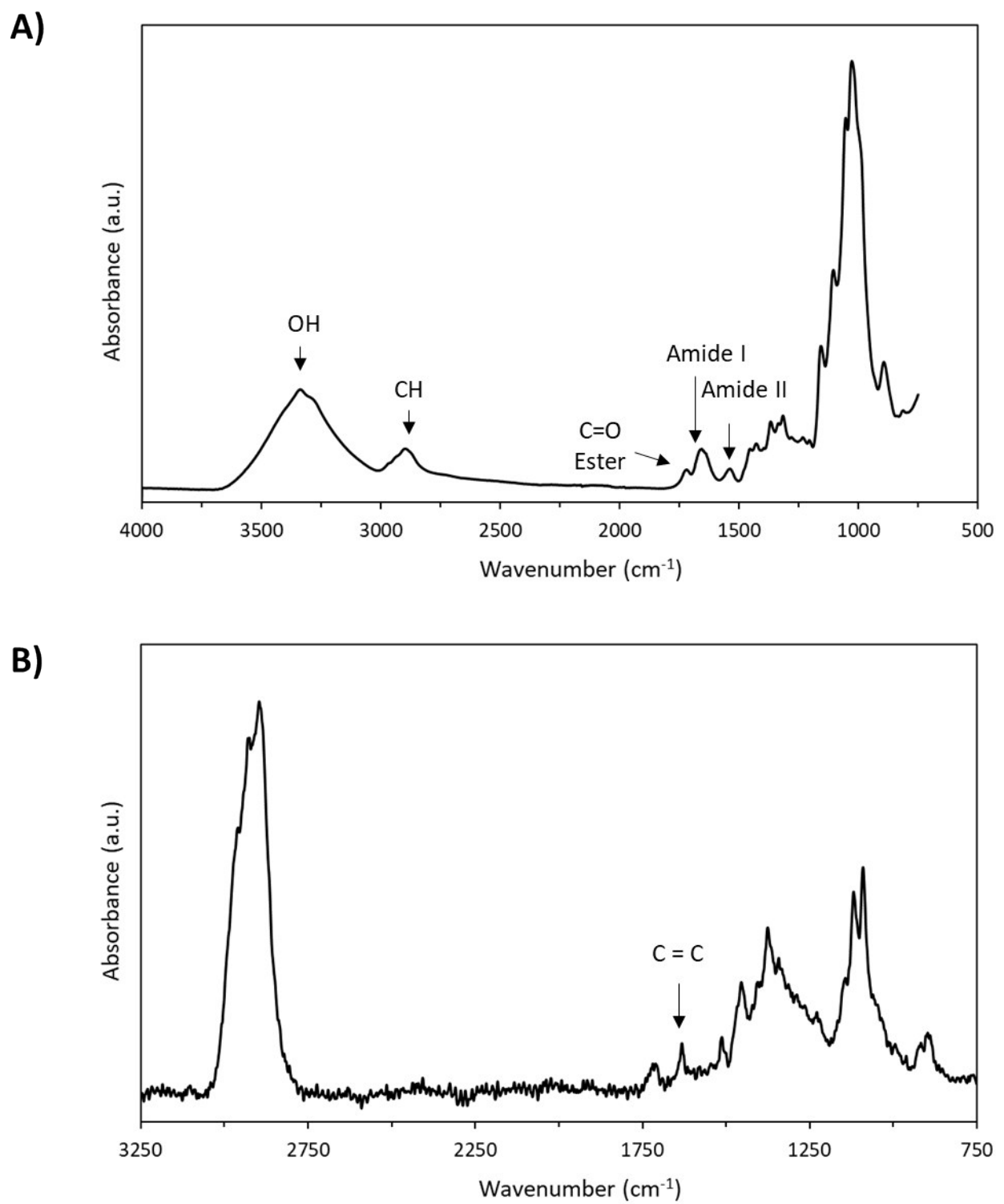


Fig. S8. A) ATR-IR, B) Raman, C) TGA and D) ^{13}C CP-MAS of Entry 7 (Table 1).



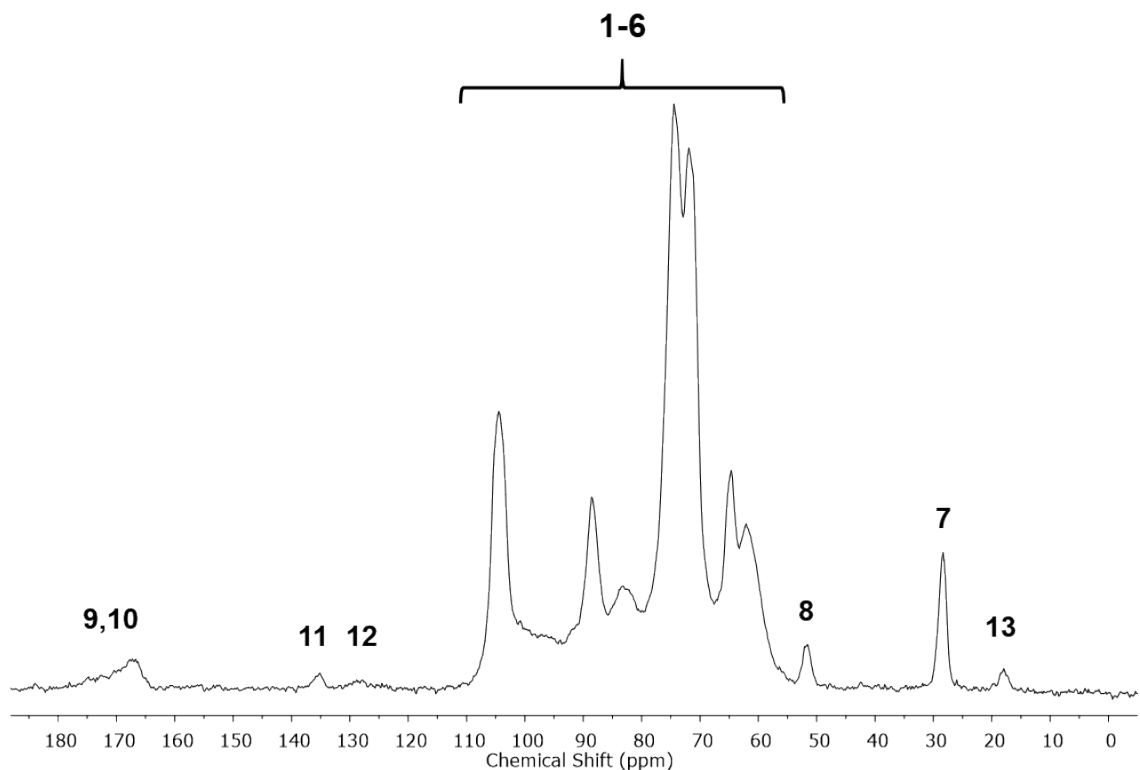
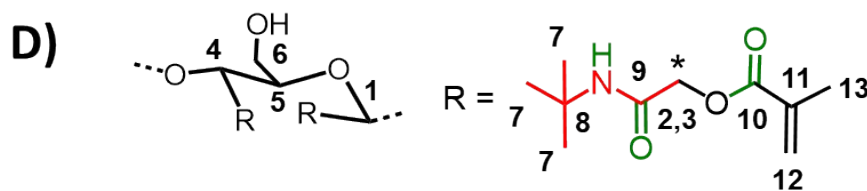
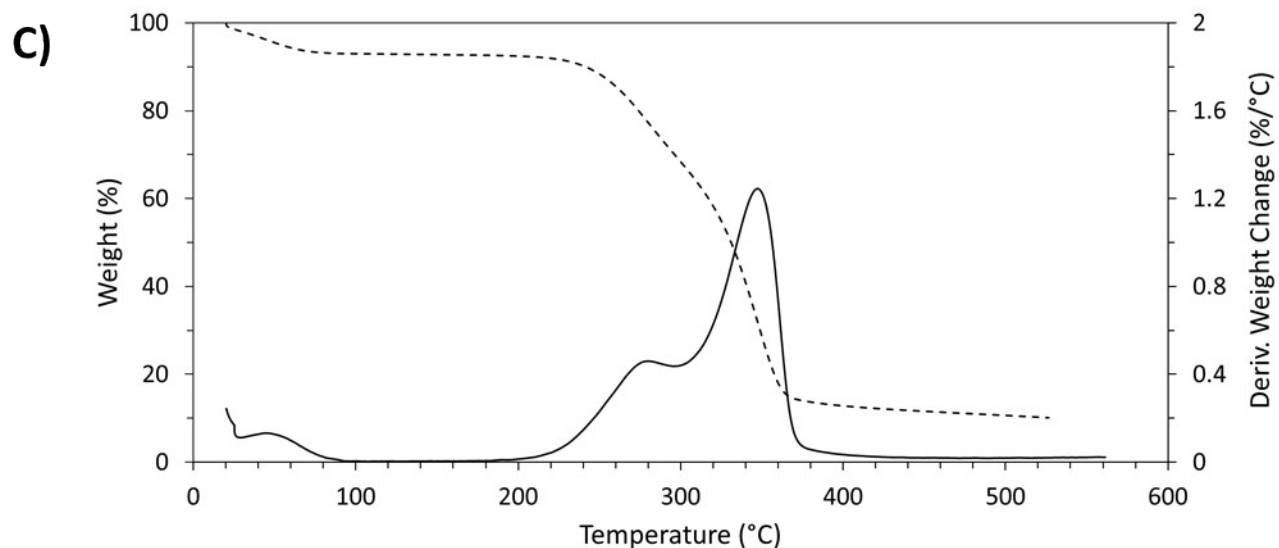
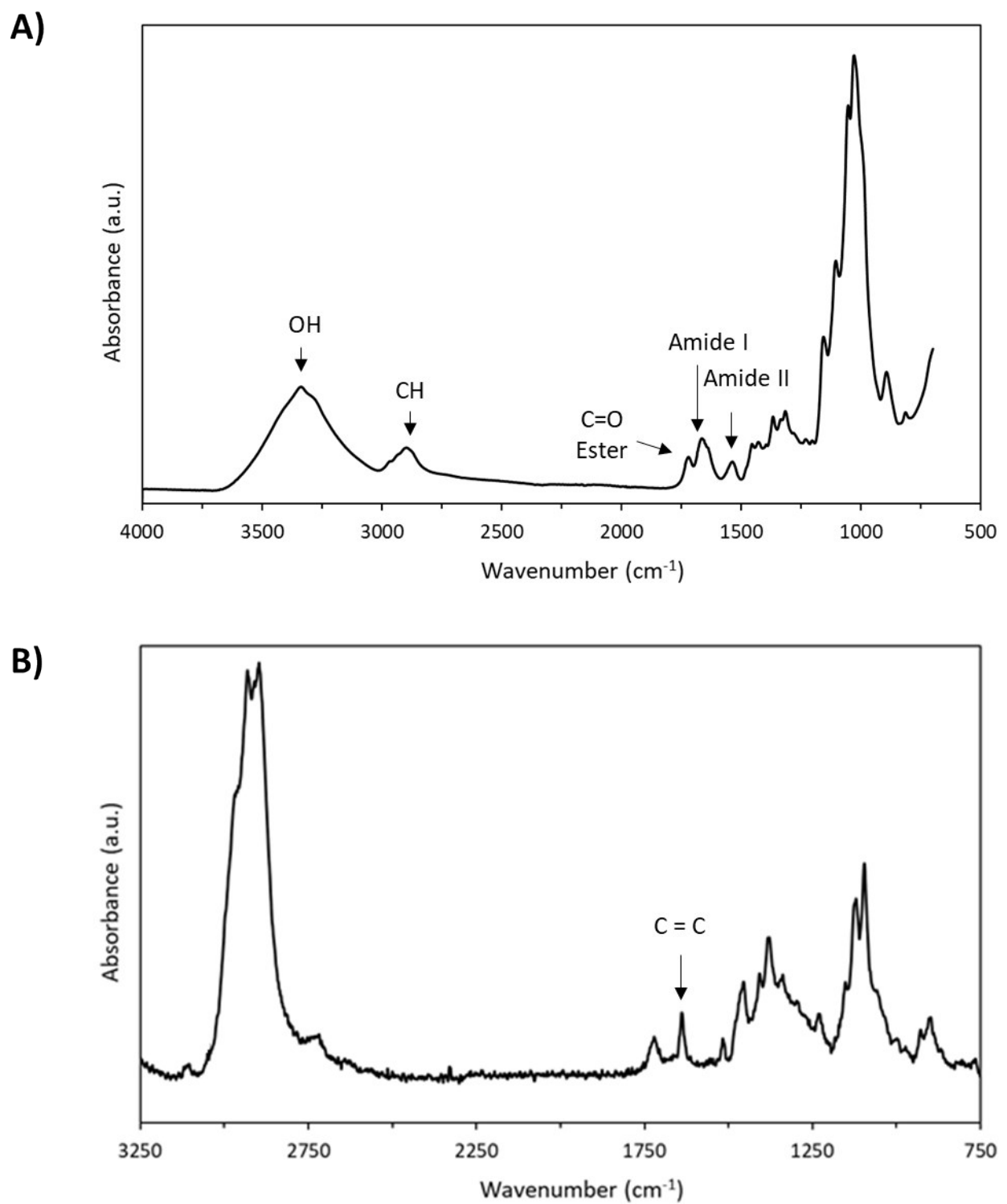


Fig. S9. A) ATR-IR, B) Raman, C) TGA and D) ^{13}C CP-MAS of Entry 8 (Table 1).



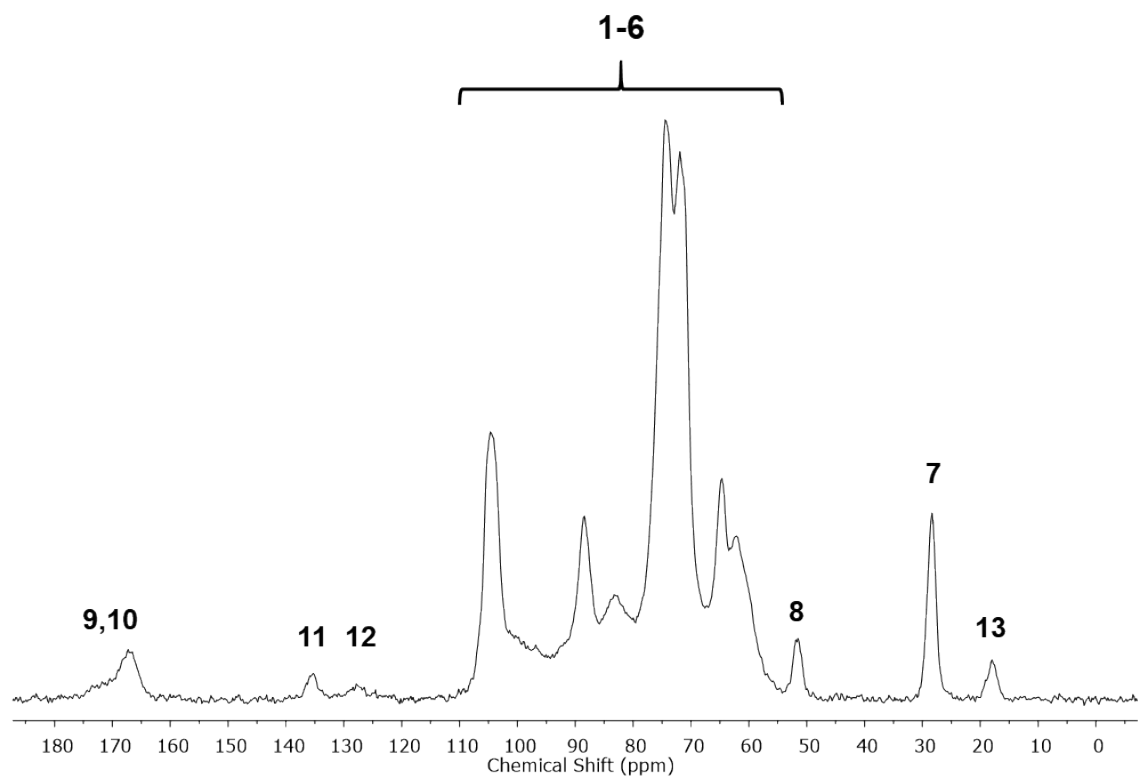
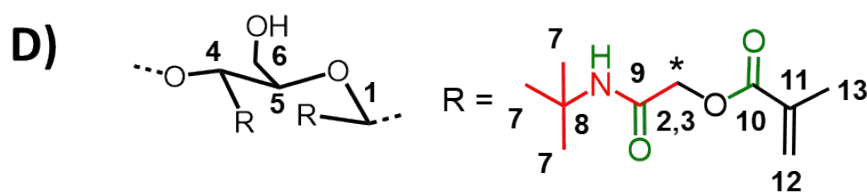
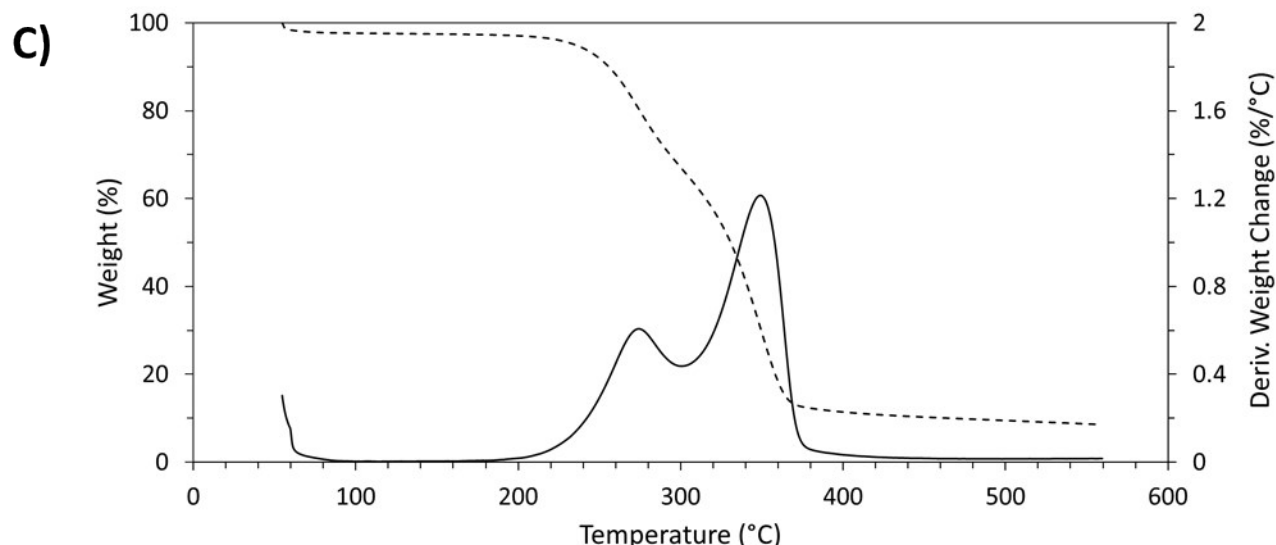
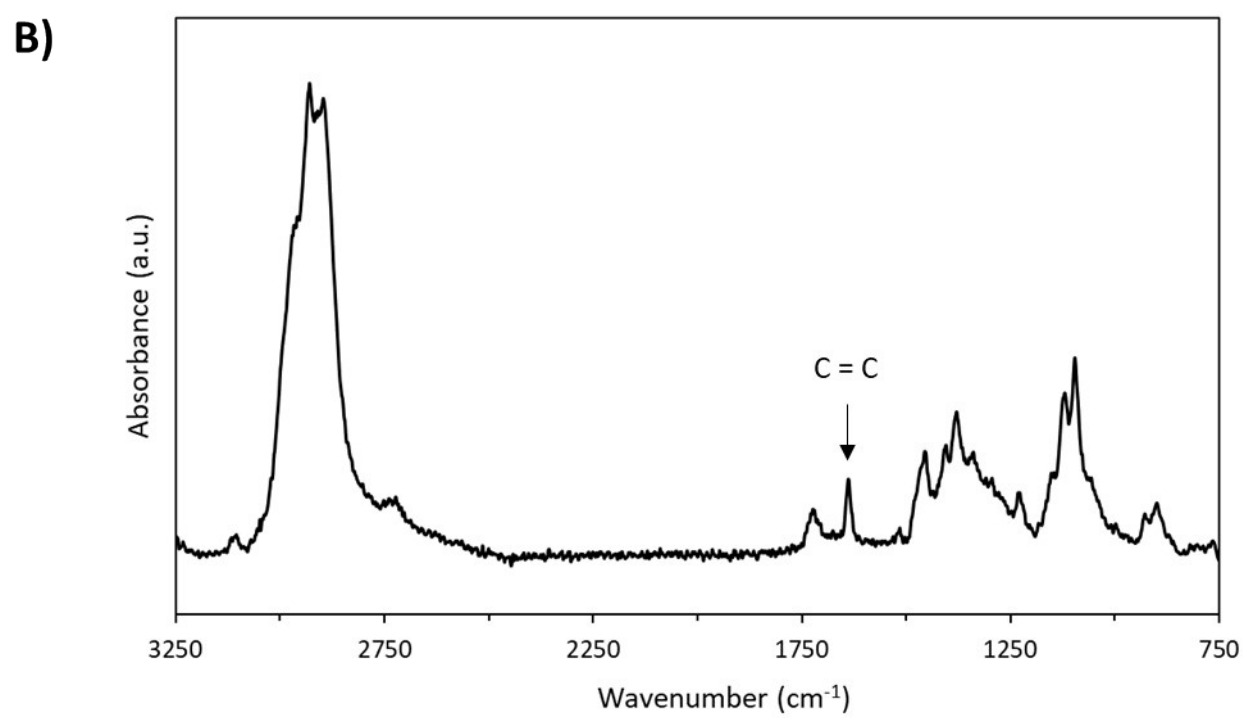
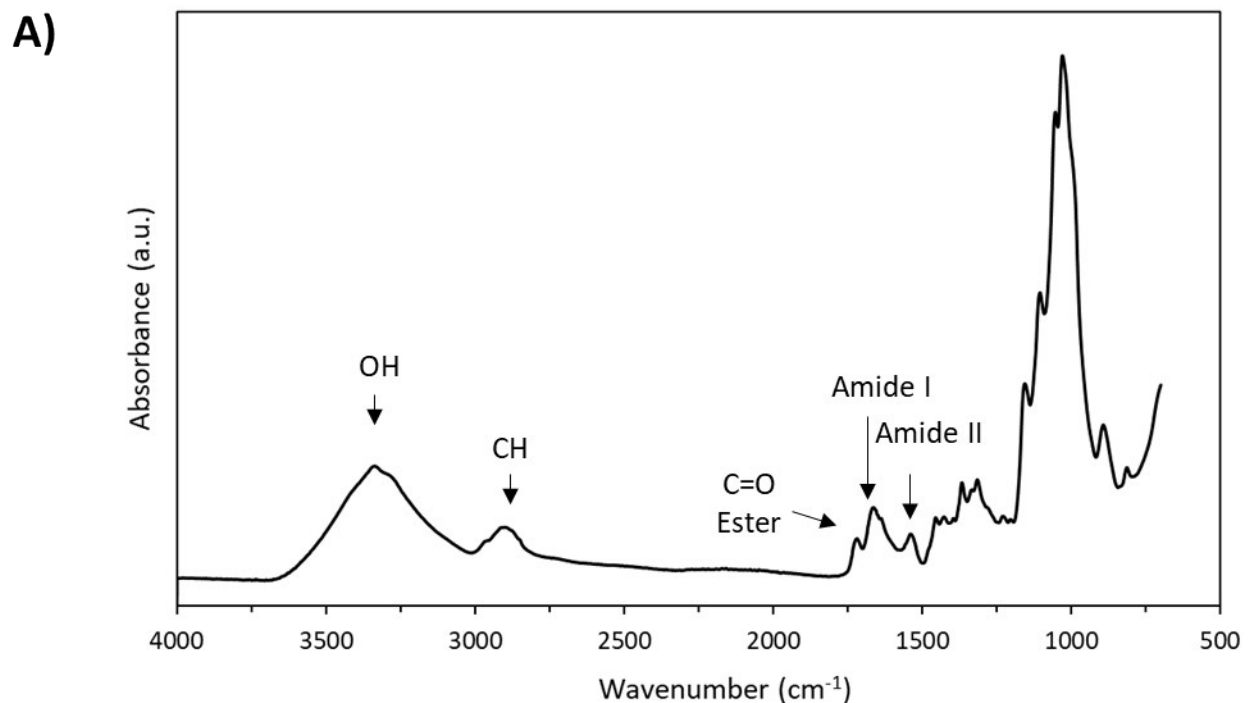


Fig. S10. A) ATR-IR, B) Raman, C) TGA and D) ^{13}C CP-MAS of Entry 9 (Table 1).



C)



D)

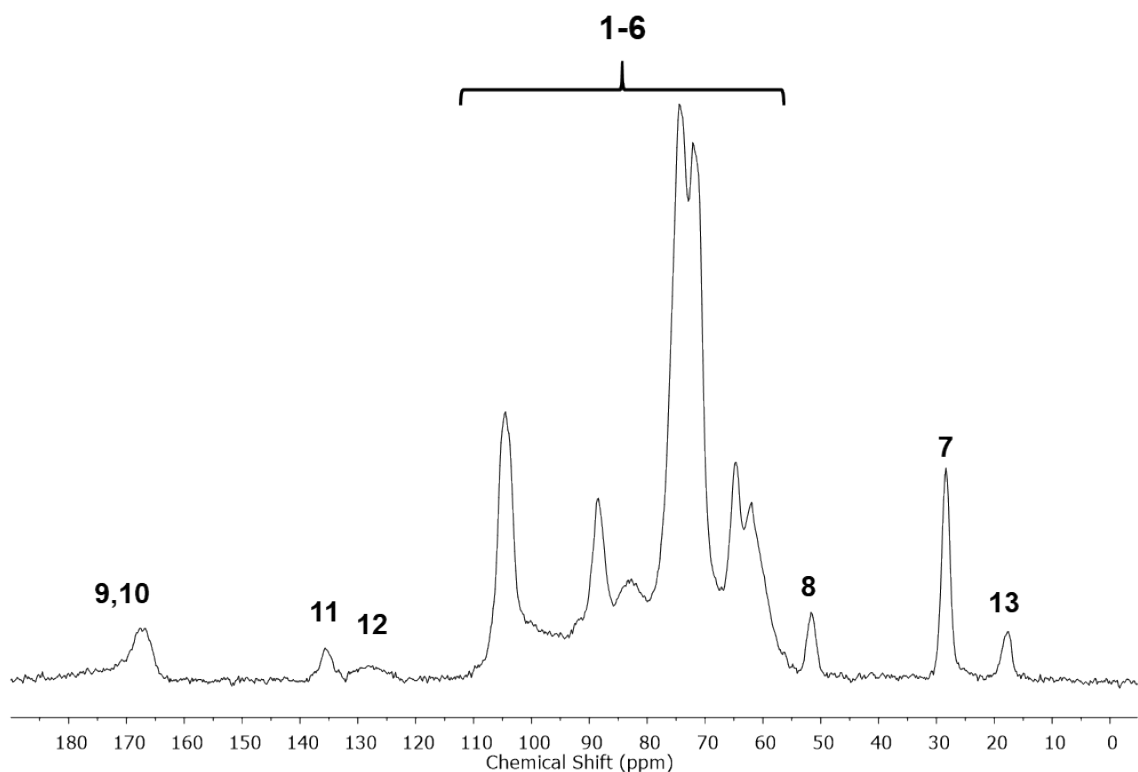
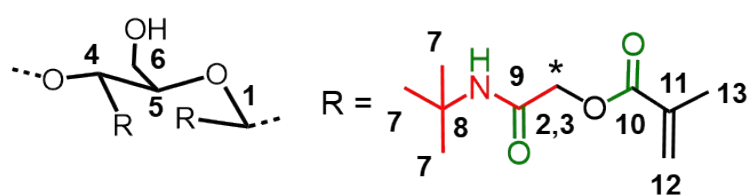
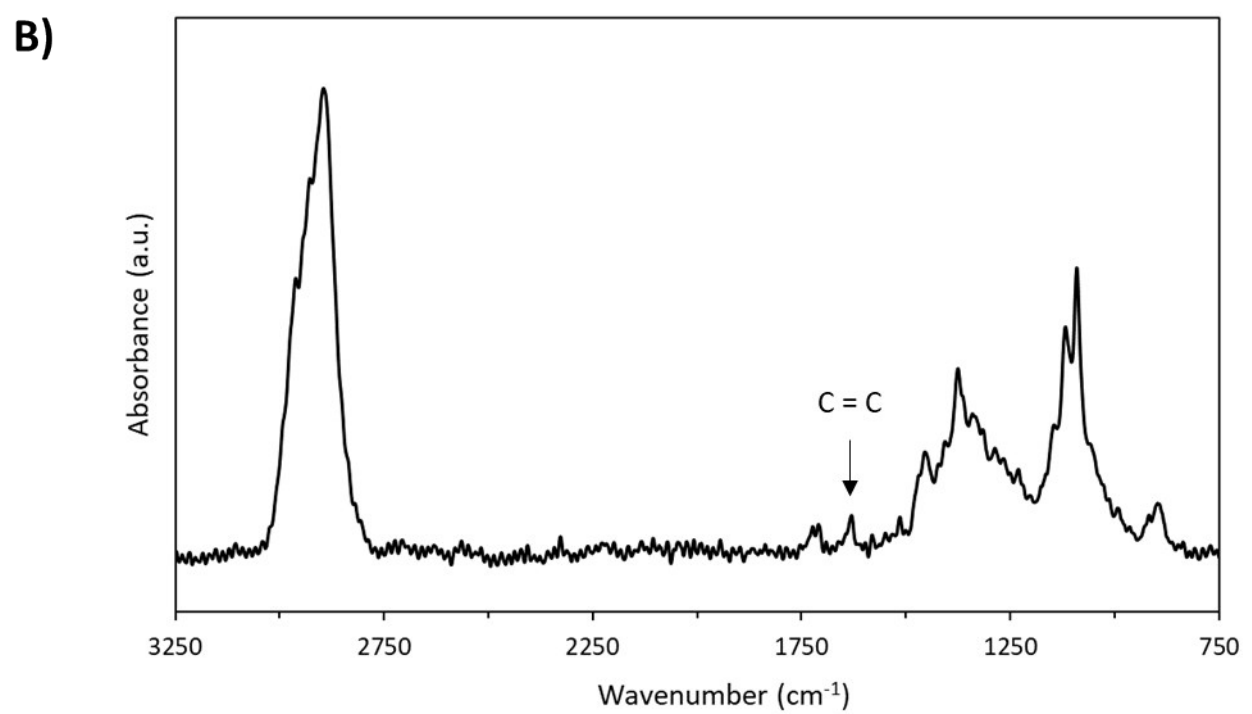
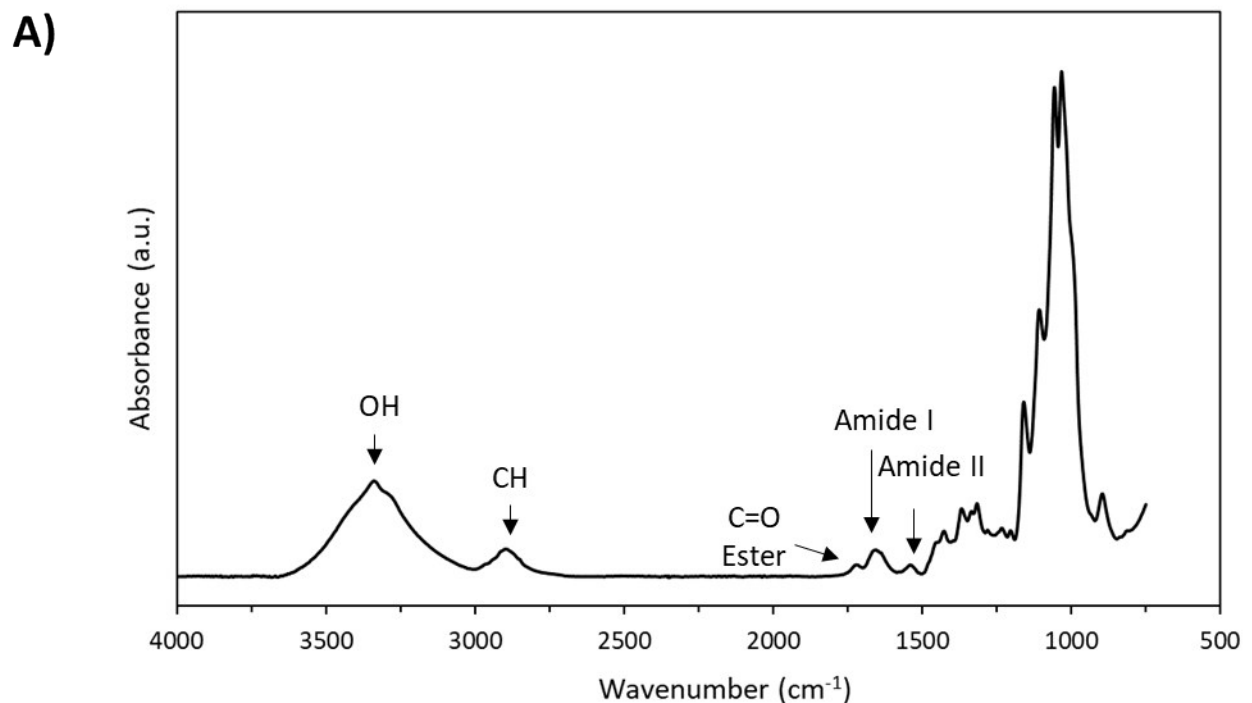


Fig. S11. A) ATR-IR, B) Raman, C) TGA and D) ¹³C CP-MAS of Entry 10 (Table 1).



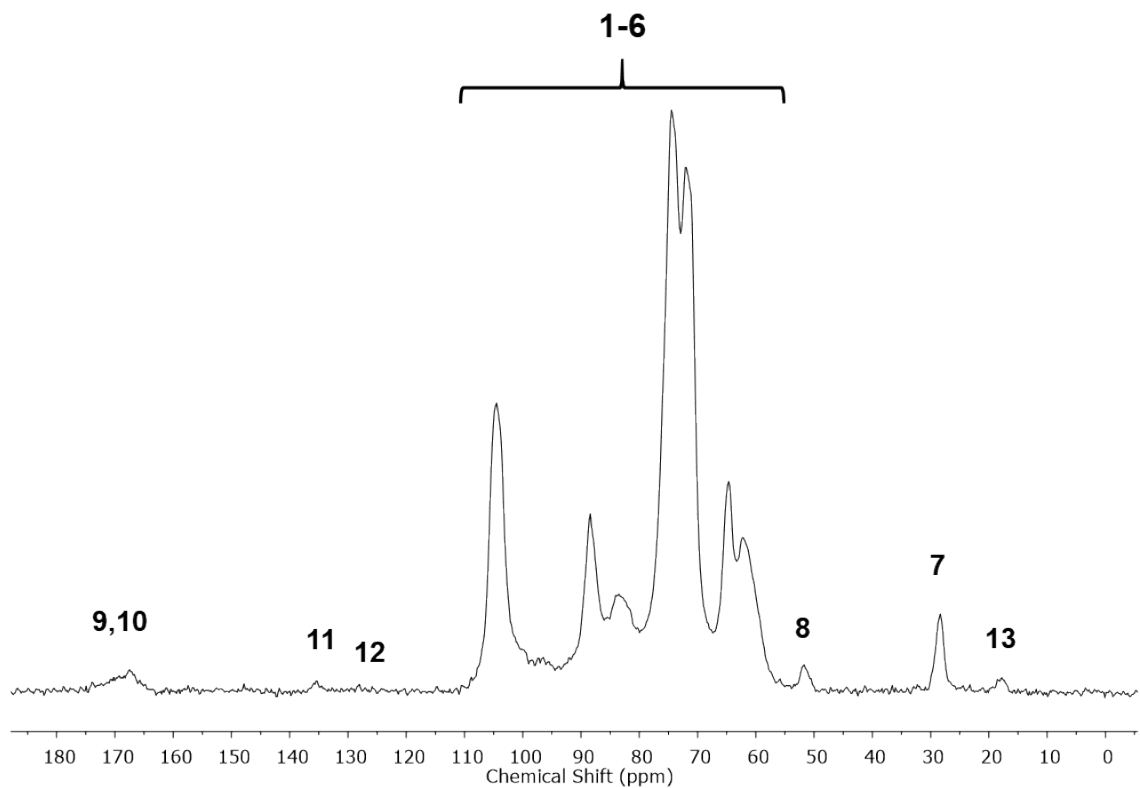
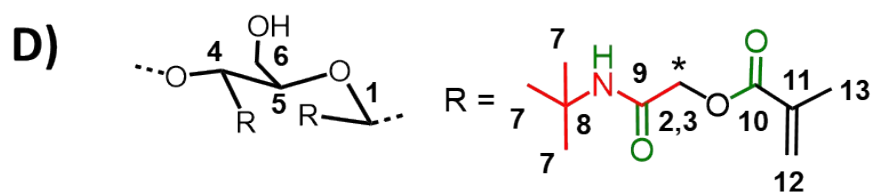
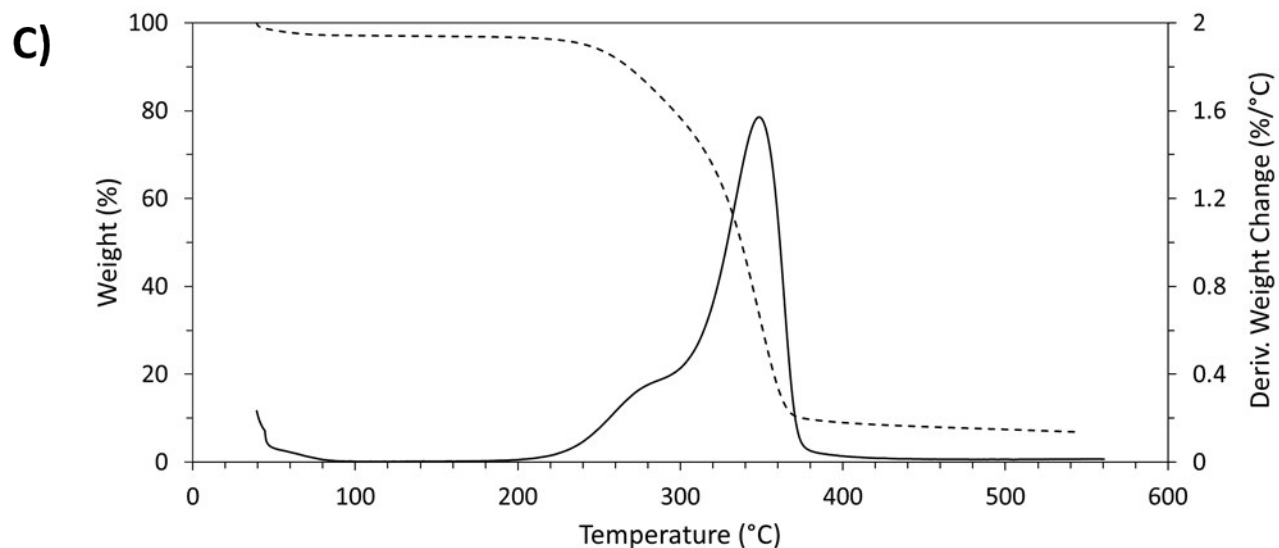
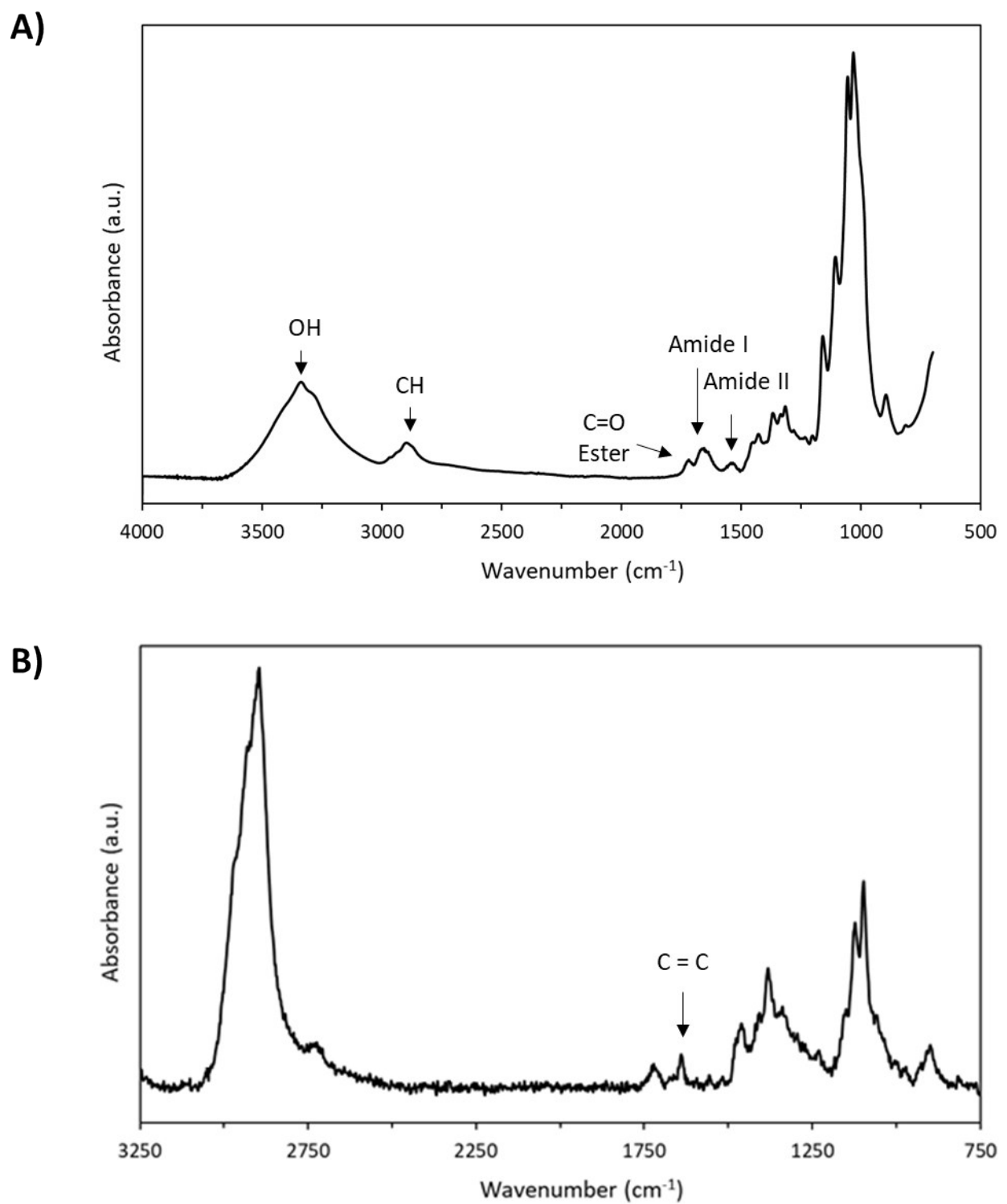


Fig. S12. A) ATR-IR, B) Raman, C) TGA and D) ^{13}C CP-MAS of Entry 12 (Table 1).



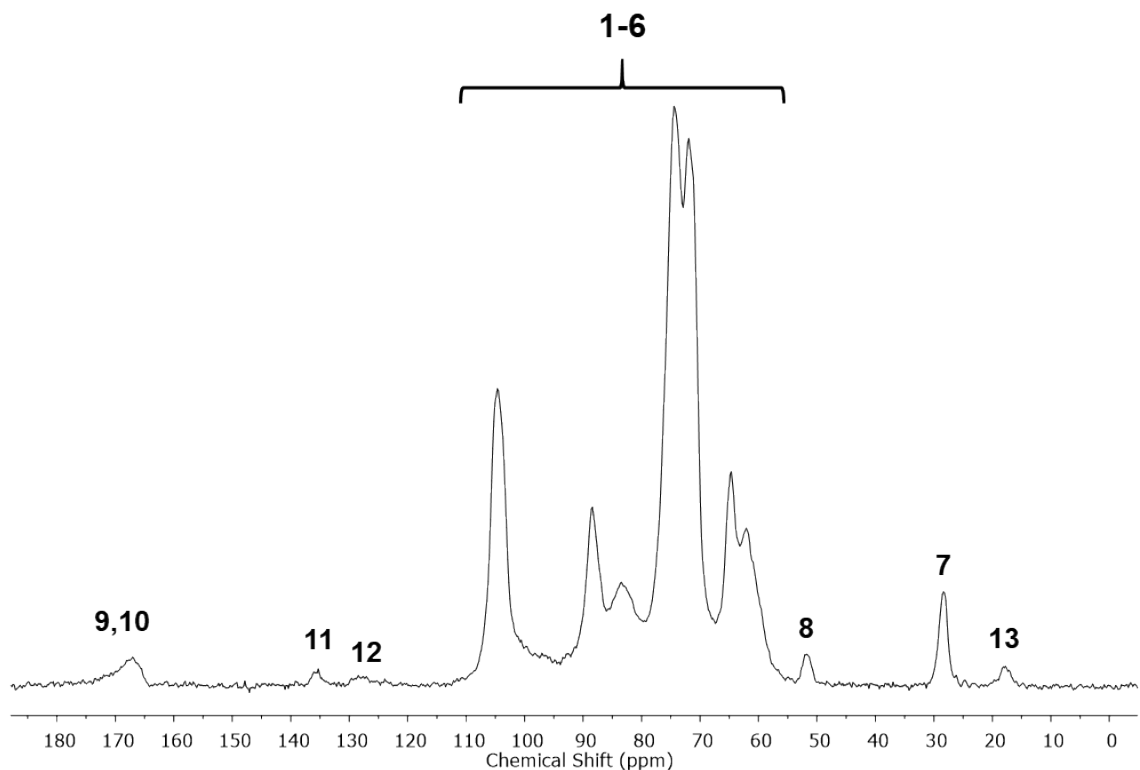
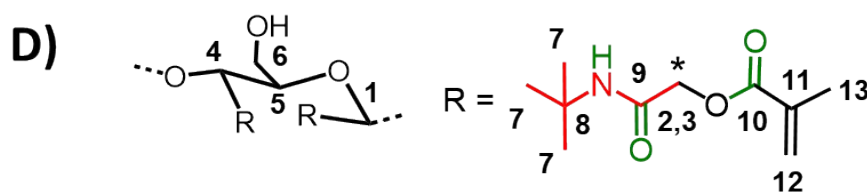
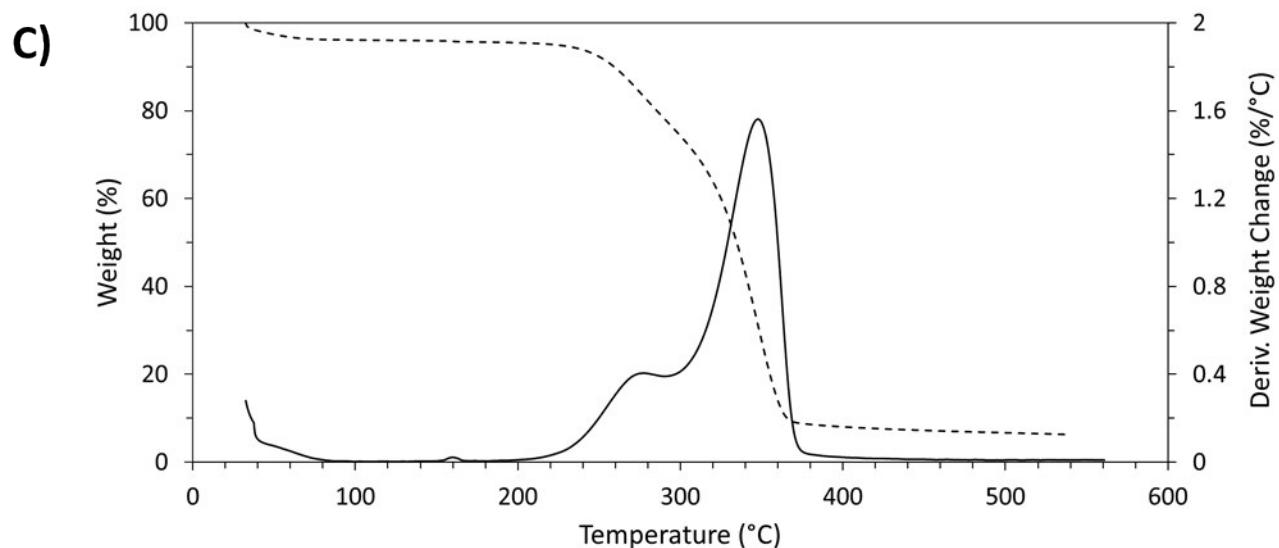
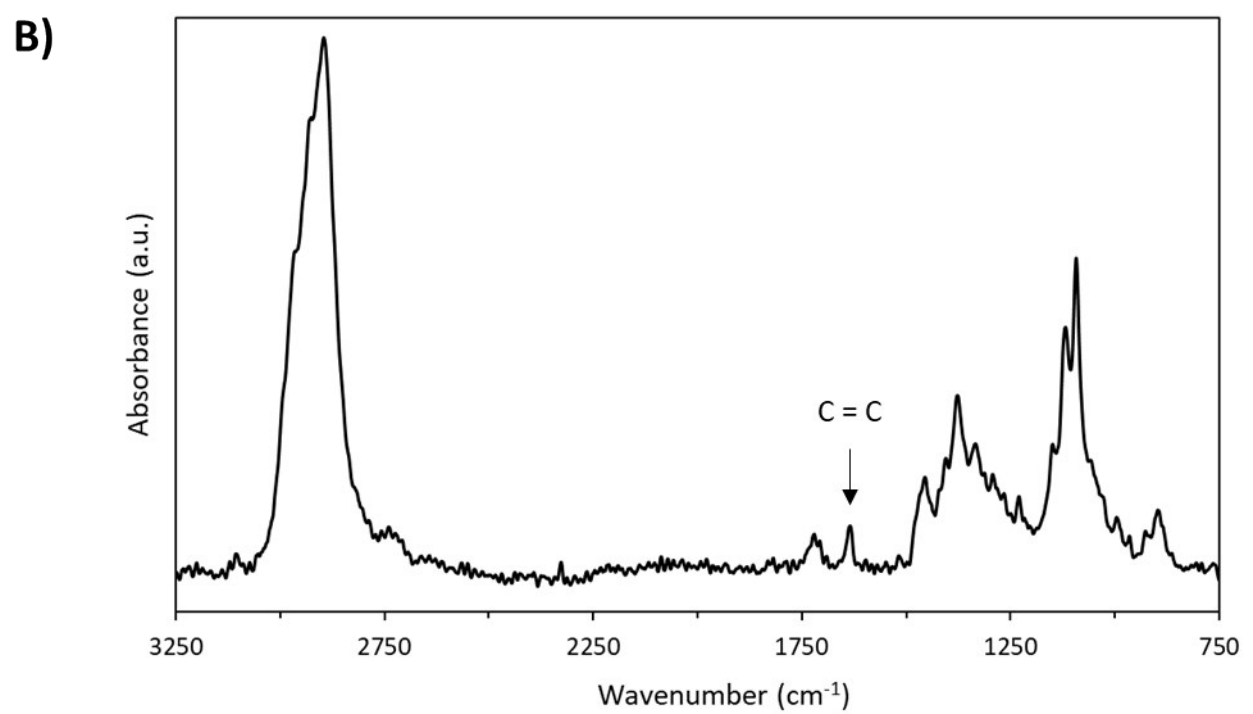
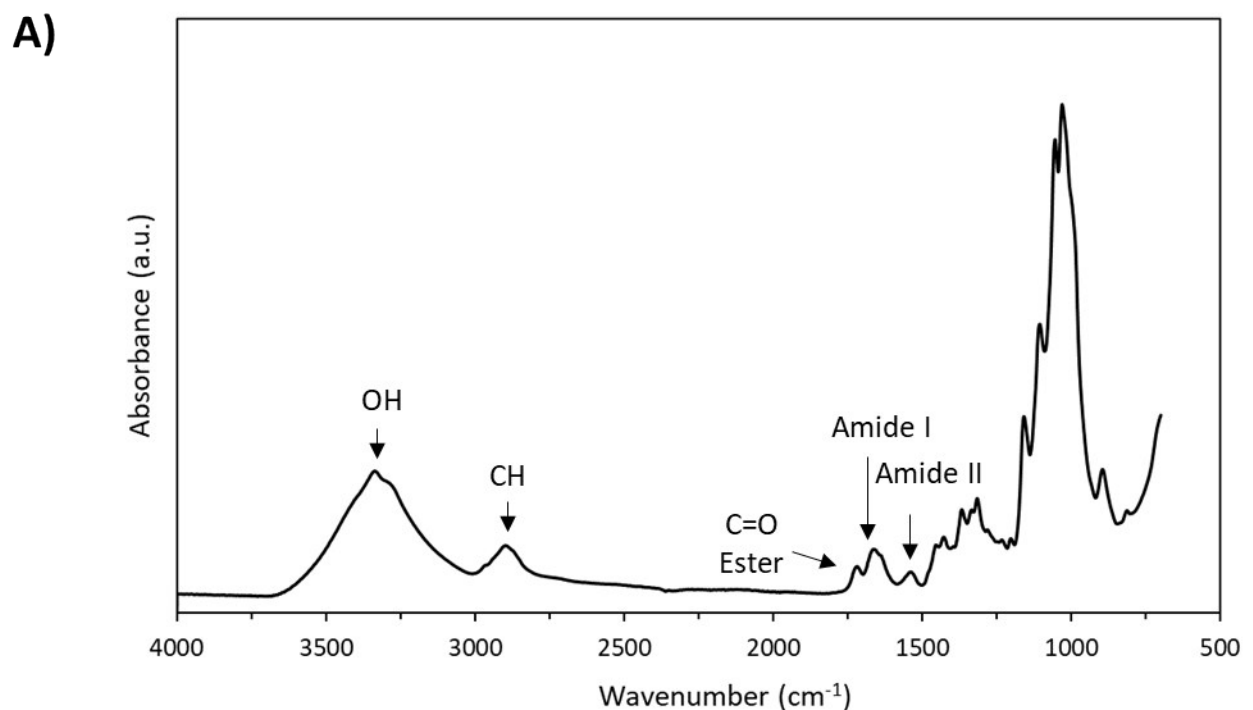


Fig. S13. A) ATR-IR, B) Raman, C) TGA and D) ^{13}C CP-MAS of Entry 13 (Table 1).



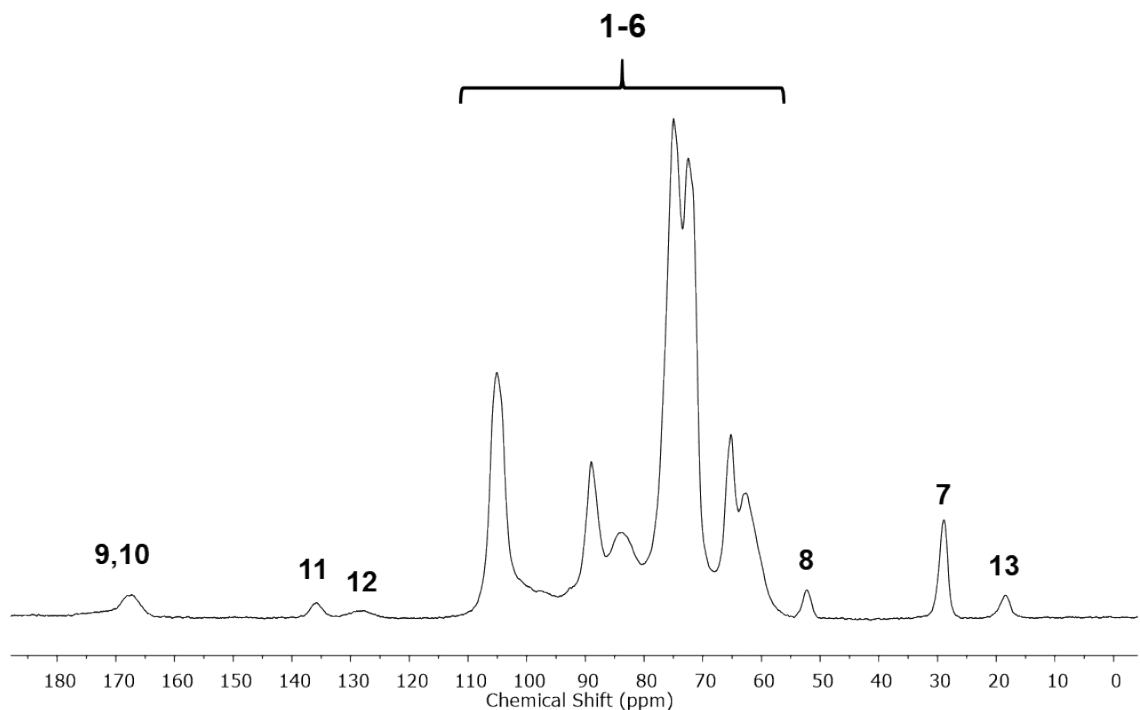
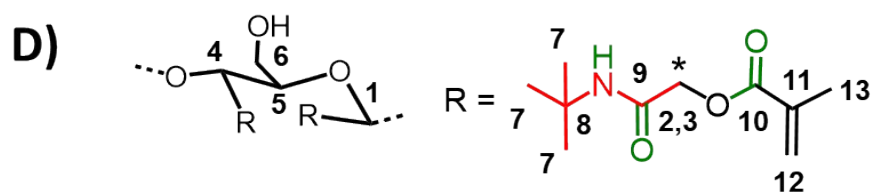
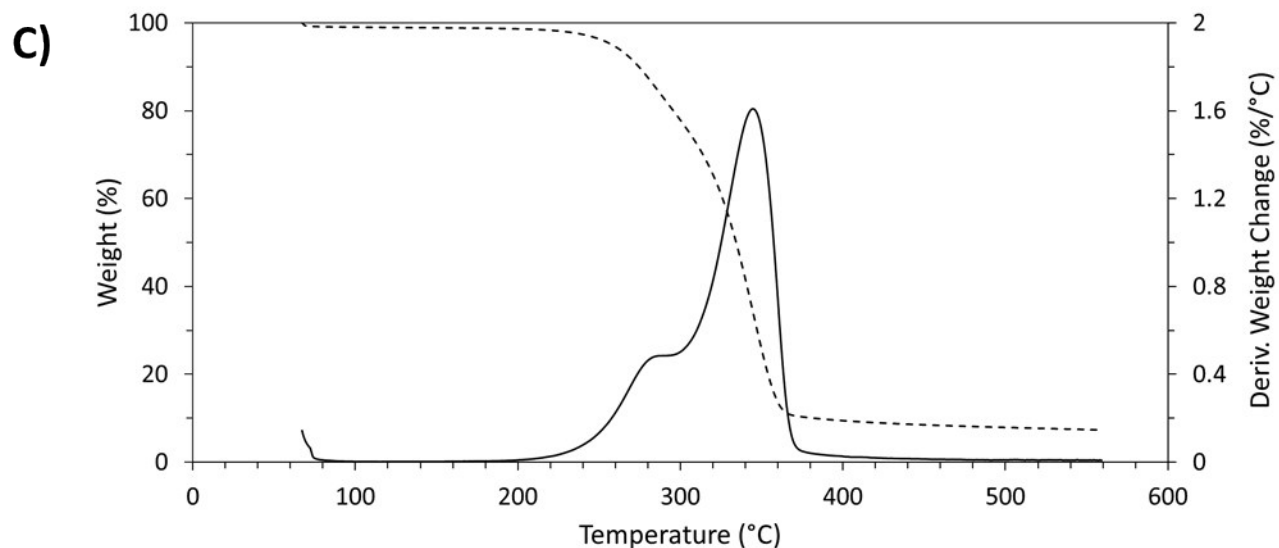


Fig. S14. A) ATR-IR, B) Raman, C) TGA and D) ^{13}C CP-MAS of Entry 14 (Table 1).

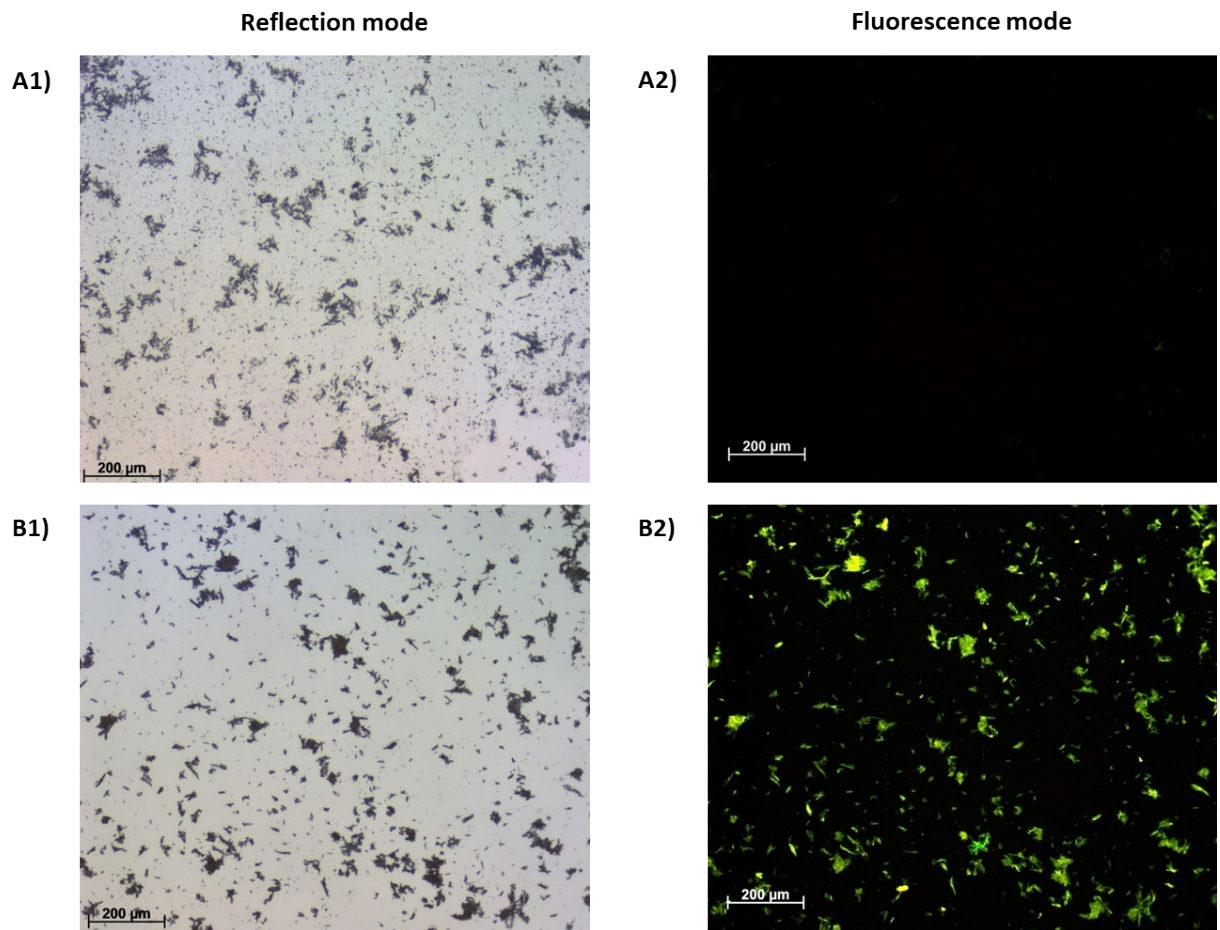


Fig. S15. Microscopy images of POC0.34-Control (A1 and B2) and POC0.34-Fluo (B1 and B2), in reflection and fluorescence mode.